

# AMORPHOUS ICES

NICOLAS GIOVAMBATTISTA<sup>1</sup>, KATRIN WINKEL<sup>2</sup>,  
and THOMAS LOERTING<sup>2</sup>

<sup>1</sup>*Physics Department, Brooklyn College of the City University of New York,  
Brooklyn, NY 11210-2889, USA*

<sup>2</sup>*Institute of Physical Chemistry, University of Innsbruck, Innrain 52a,  
A-6020 Innsbruck, Austria*

## CONTENTS



- I. Introduction
  - II. Pressure-Induced Amorphization of Hexagonal ICE: High-Density Amorphous ICE<sub>1</sub>
  - III. Low-Density Amorphous ICE<sub>2</sub>
  - IV. Apparent First-Order Transition Between Low- and High-Density Amorphous ICE
  - V. An Interpretation of Amorphous ICE Phenomenology from Computer Simulations
  - VI. Different States of Relaxation in HDA
  - VII. Very High-Density Amorphous ICE<sub>3</sub>
  - VIII. Molecular Structure of Amorphous ICES
  - IX. VHDA in Computer Simulations
  - X. The Glass-to-Liquid Transition
  - XI. Discussion
- References

## I. INTRODUCTION

Water, both in the liquid and in the solid (ice) phase, is very peculiar, with properties that differ from most substances. A growing list of currently 67 anomalous properties has been compiled by Chaplin [1]. For example, water is the only substance that can be found in nature in the solid, liquid, and gas phases [2]. In the solid phase, it can exist in a wide variety of crystalline phases. Water is also well known for its density anomalies (such as the liquid's density maximum at 277.13K and the solid's density minimum at 70K [3]), diffusion anomalies

---

*Liquid Polymorphism: Advances in Chemical Physics, Volume 152, First Edition.*

Edited by H. Eugene Stanley.

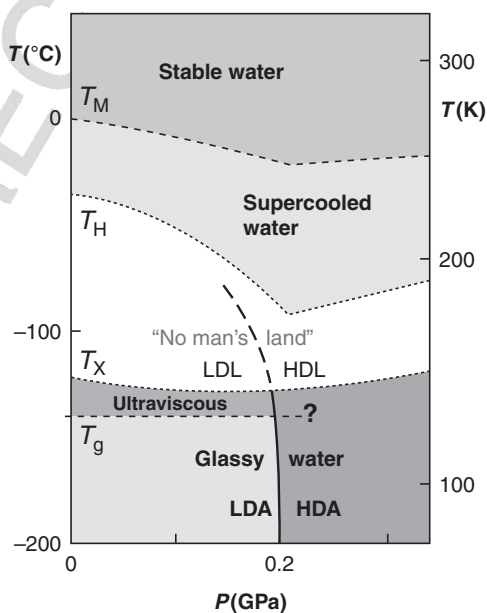
© 2013 John Wiley & Sons, Inc. Published 2013 by John Wiley & Sons, Inc.

(the increase of diffusivity upon cooling at constant pressure), and thermodynamic anomalies (such as the unusually high heat capacity at low temperatures, which shows a minimum at 309K and a maximum or apparent singularity near 228K) [2]. Many of water thermodynamic anomalies become more pronounced upon cooling below its melting point. For example, water viscosity, heat capacity, and solubility of nonpolar gases in water increase substantially below 273K, while in “normal” liquids, these properties decrease slowly upon cooling. Water anomalies are also sensitive to pressure. For example, water diffusion anomaly at 280K disappears above 0.2 GPa. For an in-depth introduction to the complexity of water, the reader is referred to Refs [2,4–10].

In order to understand why liquid water is so unusual, it seems instructive to look at the phase behavior of water at subzero temperatures. Figure 1 shows schematically the regions in the  $P$ – $T$  plane where water is found as a stable liquid, supercooled liquid (metastable), and glass or amorphous ice (metastable). Liquid water is the stable phase above the melting temperature  $T_M(P)$ . Below  $T_M(P)$ , the stable phase of water is ice; the particular stable ice phase depends on pressure and temperature (see Fig. 2). For clarity, the different ice phases are not indicated in Fig. 1.

If care is taken to avoid heterogeneous nucleation (e.g., ice formation at the container surface or induced by the presence of impurities in the sample), liquid water can be obtained below  $T_M(P)$ . This “supercooled water” can be formed at

**Figure 1.** Schematic phase diagram of noncrystalline water. Liquid water is stable above the melting temperature line  $T_M(P)$ . Below this temperature and above the homogeneous nucleation temperature  $T_H(P)$  liquid water is metastable (supercooled). The “no man’s land” is the region where crystallization cannot be avoided experimentally. Glassy water exists below the crystallization temperature  $T_X(P)$ .  $T_g(P)$  is the glass transition temperature above which glassy water becomes an ultraviscous liquid. For glassy water at 1 bar,  $T_g \sim 136\text{K}$ ; it is not clear yet what the value of  $T_g(P)$  is at high pressures (horizontal dashed line). Two different glassy forms are identified at  $P < 0.325\text{ GPa}$ , LDA and HDA. The solid line separating the LDA and HDA regions extends into the “no man’s land” (dashed line); see also Fig. 8b. Adapted from Ref. [5].



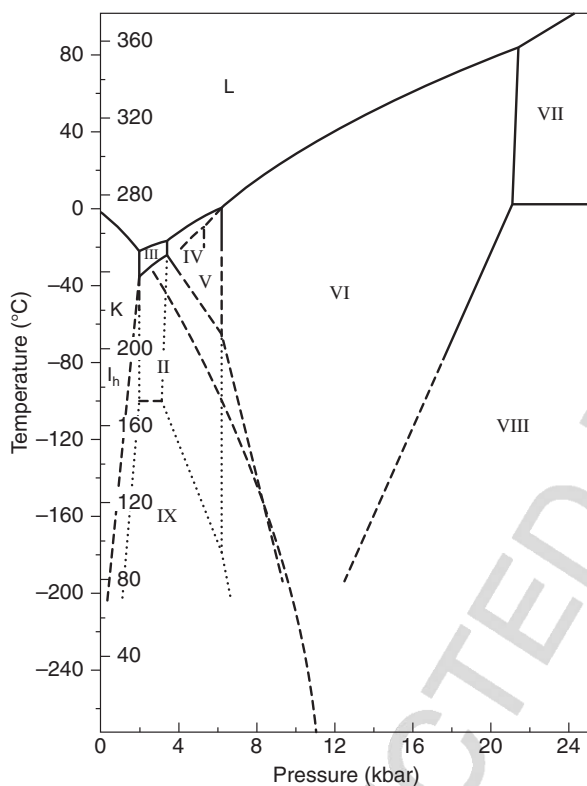


**Figure 2.** Phase diagram of ice showing the regions of stability of liquid water (L) and the regions of existence of the most common ice phases (ice  $I_h$ , and ices II-IX). Solid and dashed lines indicate the measured and extrapolated equilibrium boundaries of the different ices, respectively. Dotted lines are the metastable boundaries of the ices. The long-dashed line is an extrapolation of the ice  $I_h$  melting line to 10K. Adapted from Ref. [24].

temperatures above 231K at ambient pressure [11,12] and above 181K at 0.2 GPa [13]. However, even if heterogeneous nucleation is perfectly avoided in experiments, ice forms rapidly at temperatures below the homogeneous nucleation temperature  $T_H(P)$ .

The “phase diagram” of noncrystalline water would end at  $T_H(P)$  if it was not for the existence of amorphous ices, the main focus of this chapter. These amorphous ices can form under suitable conditions at temperatures below the crystallization line  $T_X(P)$  (see Fig. 1). Classically, glasses or amorphous solids are defined as solids with no long-range order. It is often suggested that “amorphous solids” represent the low-temperature, kinetically immobilized (vitrified) liquid. This requires that amorphous ices are thermodynamically continuously connected with a liquid, that is, glasses experience a reversible glass-liquid transition [14]. It is important to distinguish between glasses and “nonglassy amorphous solids.” Nonglassy amorphous solids are amorphous materials (as, e.g., characterized by X-ray diffraction patterns) that may contain very small crystallites or may even be composed entirely of such crystallites. While glasses experience a reversible

glass-to-liquid transition, “nonglassy amorphous solids” rather ~~recrystallize and show no~~ glass-to-liquid transition. A glass-to-liquid transition may be hard to detect experimentally and so its ~~absence~~ is no proof for a nonglassy nature [15].

When glassy water, formed at  $T \ll T_X(P)$  and low pressures, is heated, it transforms to a very viscous liquid at  $T \sim T_g(P)$  (see Fig. 1).  $T_g(P)$  is known as the glass transition temperature and indicates approximately the temperature above which the relaxation time of the liquid becomes smaller than the characteristic timescale of the experiment. As such, the specific value of  $T_g(P)$  is not unique and can depend on experimental details, such as the particular heating rates used in the experiment. Whereas melting occurs at the well-defined temperature  $T_M(P)$ ,  $T_g(P)$  represents a more or less narrow temperature range. The structural relaxation time changes by  $\sim 2.3$  orders of magnitude from the onset of the glass transition to its end. At  $T_g$  ~~observed by~~ differential scanning calorimetry (DSC) with  $10\text{K min}^{-1}$  cooling rate, viscosity is about  $10^{12}$  Pa s ( $10^{13}$  poise), and structural relaxation time is about 100 s. For glassy water at  $P = 1$  bar,  $T_g \sim 136\text{K}$  (Fig. 1). It is not clear yet what the value of  $T_g$  is at high pressures.

If glassy water is heated above  $T_X(P)$ , it rapidly crystallizes. Thus, at temperatures  $T_X > T > T_H$  only crystalline ice can be observed experimentally (on the timescale of milliseconds or longer). Therefore, metastable (supercooled or glassy) water remains unexplored in experiments of *bulk* pure water. This region is denoted as “No man’s land” in Fig. 1 [5]. An experimental characterization is possible only with ultrafast methods, which are experimentally so demanding that they have so far not successfully been employed for measuring liquid water properties in this temperature range. Instead, computer simulations have been the sole means of investigating bulk water in the “No man’s land.” Although it has been proposed that liquid water can be studied in the “No man’s land” in nanoconfined environments [16,17] or in the vicinity of interfaces [18,19], it is not so clear what effect the confinement or interface has on water properties [20].

Water is also anomalous in the glass state since it can exist in more than one glass state at  $T < T_X(P)$ , a property known as “amorphous polymorphism” or “polyamorphism.” In Fig. 1, two amorphous ices are indicated at  $P < 0.325$  GPa, namely, high-density amorphous ice (HDA) and low-density amorphous ice (LDA). At high pressures ( $P > \sim 0.8$  GPa), glassy water even exists as a third distinct amorphous state, namely, very high-density amorphous ice (VHDA) [21]. In this work, we focus on water phenomenology at  $T < T_X(P)$ . We discuss the phenomenology associated with HDA and LDA in Sections II and III, respectively, and discuss the nature of the transformation between LDA and HDA in Section IV. In Section V, we discuss results from computer simulations that provide a potential phase diagram for metastable water in the “No man’s land,” characterized by a second critical point (CP) ( $C'$ ). The relaxation state of HDA and the difference between “unannealed” and “expanded” HDA are discussed in Section VI. VHDA is discussed in Section VII and the structure of VHDA, as well as the structure of LDA and HDA,

is described in Section VIII. A brief discussion of the results obtained from computer simulations is presented in Section IX. We summarize the current knowledge about the glass-to-liquid transition in amorphous ices in Section X. In Section XI, we address the frequently asked question “How many amorphous ices are there?” [21] and discuss the relationship among them.

## II. PRESSURE-INDUCED AMORPHIZATION OF HEXAGONAL ICE: HIGH-DENSITY AMORPHOUS ICE

The phase diagram of water including its crystalline phases is very unusual. Figure 2 indicates the presence of nine different ices at  $T > 100\text{K}$ . In fact, there are at least 16 different forms of crystalline ice reported up to date [22,23]. In 1984, Mishima et al. [24] performed experiments at very low temperature with the goal of exploring the phase diagram of ice well below  $T_g$ . In their experiments, hexagonal ice ( $I_h$ ) was compressed at constant temperature  $T = 77\text{K}$ . What they found was surprising. Instead of observing a transformation of ice  $I_h$  to another crystalline phase, such as ice IX, they found that ice  $I_h$  transforms to an amorphous solid when the sample pressure reaches  $\sim 1\text{ GPa}$ . Due to the high density of the resulting amorphous ice, approximately  $1.31\text{ g cm}^{-3}$  at  $T = 77\text{K}$  and  $P \sim 1\text{ GPa}$ , this amorphous solid was named HDA. These experiments were relevant not only for our understanding of ice but also for the understanding of low-temperature materials in general. Mishima et al. showed, for the first time, that an amorphous solid could be formed by isothermal compression of a crystal, a process that nowadays is commonly known as pressure-induced amorphization (PIA). Since then, amorphous solids formed by PIA of crystals have been obtained in different substances [25] such as  $\text{GeO}_2$  [26],  $\text{GeSe}_2$  [27], Si [28], and quartz [29].

The typical evolution of the piston displacement with pressure  $d(P)$  upon compressing a sample of ice  $I_h$  at  $T = 77\text{K}$  to  $P \sim 1.5\text{ GPa}$  is shown in the lower panel of Fig. 5 [24]. The sharp change in  $d(P)$  at  $P \sim 1.0\text{ GPa}$  corresponds to the ice  $I_h$ -to-HDA transition (further compression of HDA above  $P \sim 4\text{ GPa}$  results in a crystalline phase close in structure to ice VII or VIII [30,31]). The sharpness of the ice  $I_h$ -to-HDA transformation, reminiscent of a first-order transition, is quite unusual. For comparison, ice IX at  $T = 77\text{K}$  does not transform when compressed to  $P = 2.5\text{ GPa}$  even when it is metastable relative to ice II, and becomes metastable relative to ice VI and VIII at high pressures (see Fig. 1) [24]. The experiments reported in Ref. [24] also indicate that the ice  $I_h$ -to-HDA transition cannot be reversed (see lower panel of Fig. 5) by simply decompressing. It is difficult for the crystal to nucleate from the amorphous ice at such a low temperature. Instead, releasing the pressure results in *recovered* HDA of density  $1.17\text{ g cm}^{-3}$  at  $T = 77\text{K}$  and 1 bar, 24% larger than the density of ice  $I_h$  at same conditions ( $0.94\text{ g cm}^{-3}$ ). A summary of densities of amorphous and crystalline ice samples as measured

using the method of cryoflotation can be found in Ref. [32]. The X-ray pattern of recovered HDA at 1 bar is reported in Ref. [24]. It shows a broad halo peak at  $\sim 3.0 \text{ \AA}$ , indicating that the sample is indeed noncrystalline.

Two interpretations of the ice  $I_h$ -to-HDA transition have been proposed. This transition was first interpreted as “melting” of ice to a vitrified liquid [24,33]. This interpretation is based on the fact that the melting line of ice  $I_h$ , at  $T > 250\text{K}$  and  $P < 0.2 \text{ GPa}$ , has an unusual negative slope (Figs. 1 and 2). This implies that ice  $I_h$  can be melted by isothermal compression at  $T > 250\text{K}$ . By analogy, if ice  $I_h$  was compressed below water’s  $T_g$ , ice  $I_h$  could still “melt” not ~~only~~ to a liquid but ~~also~~ to a vitrified liquid. In fact, an extrapolation of the ice  $I_h$  melting line to  $P = 1 \text{ GPa}$  (long-dashed line in Fig. 1) results in a melting temperature  $T \sim 77\text{K}$ , very close to the temperature and pressure at which the ice  $I_h$ -to-HDA transition occurs. In this view, HDA is the amorphous ice that one obtains upon cooling liquid water below  $T_g$  at  $P > 1 \text{ GPa}$  (see Ref. [34]). An alternative interpretation of the ice  $I_h$ -to-HDA transition was proposed in Refs [35,36] and suggests that HDA is mechanically collapsed ice  $I_h$ . Thus, in this alternative view, HDA is not necessarily related to the liquid phase and, therefore, would differ from the amorphous ice formed upon fast cooling liquid water at  $P > 1 \text{ GPa}$ .

Isobaric compression of ice  $I_h$  at  $165 < T < 250\text{K}$  [37–39] results in crystallization to other phases (e.g., ices II and III) [40] and neither liquid nor amorphous ice can be formed in *pure ice* experiments. This is the main problem in understanding the relationship between the ice  $I_h$  melting line, at  $T > 250\text{K}$ , and the amorphization line, at  $T \sim 77\text{K}$ . One way to avoid ~~recrystallization~~ of ice  $I_h$ , is to use *emulsified ice* [13]. In this emulsion, water is mixed with different solutes and cooled at low temperature. The resulting ice emulsion consists of ice  $I_h$  domains confined in droplets with radius of  $1\text{--}10 \mu\text{m}$ . Such small volumes suppress ~~recrystallization~~ of ice upon isothermal compression and the melting and amorphization lines obtained upon isobaric compression of emulsified ice  $I_h$  can be traced at all temperatures [37].

Figure 3 shows the melting/amorphization lines obtained with emulsified ice [37]. Above  $T_H(0.2 \text{ GPa}) \sim 190\text{K}$ , isothermal compression of emulsified ice  $I_h$  results in melting to a supercooled (metastable) liquid. The melting line obtained with the emulsified ice extrapolates smoothly with the melting line of pure ice at  $T > 250\text{K}$ . On the other extreme, below  $T \sim 150\text{K}$ , emulsified ice  $I_h$  transforms to HDA. The amorphization line obtained with the emulsified ice coincides with the amorphization line obtained with pure ice  $I_h$ . At intermediate temperatures,  $\sim 150 \leq T \leq \sim 190\text{K}$ , a supercooled liquid or amorphous ice is observed as an intermediate state, before emulsified ice  $I_h$  transforms to high pressure ices. The results of Ref. [37] indicate that the melting and amorphization lines connect smoothly with a crossover at  $T \sim 160\text{K}$ . This crossover temperature,  $T \sim 160\text{K}$ , coincides with the estimated glass transition temperature of HDA at  $P \sim 0.5 \text{ GPa}$  (see Section IX) [41].

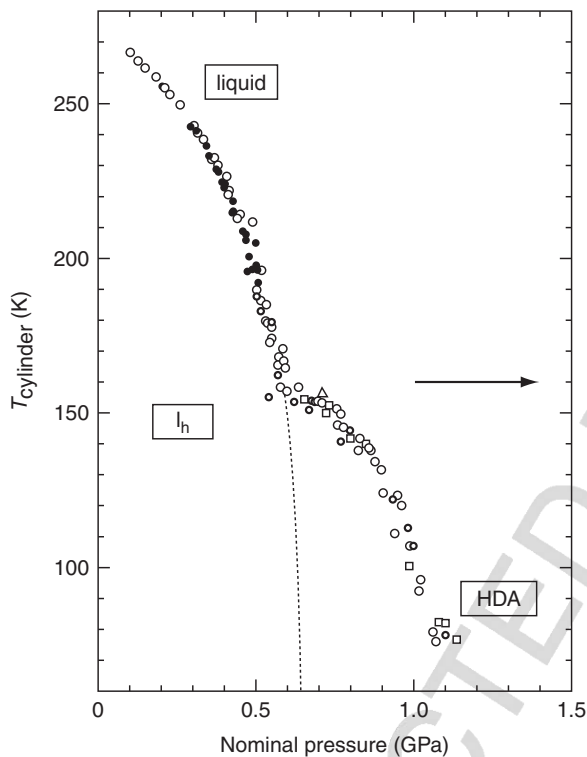


**Figure 3.** The relationship between the melting and amorphization lines of emulsified ice  $I_h$ . The dotted line is the extrapolation of the melting line of emulsified ice  $I_h$  (at  $T > \sim 170\text{K}$ ) and is an improved version of the long-dashed line shown in Fig. 2. The data points indicate a smooth crossover from equilibrium melting to sluggish amorphization at  $T \sim 140\text{--}160\text{K}$ . The arrow indicates the glass transition temperature of HDA at  $P \sim 0.5\text{ GPa}$ ,  $T_g \sim 160\text{K}$ , from Ref. [41]. The amorphization data points, at  $T < 140\text{K}$ , clearly deviate from the extrapolated melting line at low temperatures. Filled, empty, and two concentric circles correspond to ice emulsion samples; empty squares represent data from pure bulk ice samples. Adapted from Ref. [37].

Figure 3 shows that the ice  $I_h$ -to-HDA amorphization line at  $T < \sim 130\text{K}$ , deviates from the extrapolation of the melting line at low temperatures. Therefore, the results of Ref. [37] suggest that HDA, obtained by PIA of ice  $I_h$  at  $T < \sim 130\text{K}$ , is the result of a mechanical instability of the ice  $I_h$  and, thus, is different than the amorphous ice that would be formed by quenching the liquid at high pressure. The HDA formed at  $T < \sim 130\text{K}$  by PIA has been called u-HDA (unrelaxed HDA) [42]. The experiments of Ref [37] also show large structural changes in the HDA samples obtained at  $T \sim > 130\text{K}$ . The connection between the amorphous ice obtained by PIA at  $T > \sim 130\text{K}$  and the liquid phase are not fully understood. We will address this issue in Sections VI–IX.

### III. LOW-DENSITY AMORPHOUS ICE

If HDA, recovered at  $T = 77\text{K}$  and 1 bar, is heated at constant pressure then a transformation to a second amorphous ice occurs at  $T_{\text{HDA-LDA}} \sim 117\text{K}$  (for a heating rate of  $2.6\text{K min}^{-1}$ ) [24,43–46]. This new amorphous ice has a density of

$\sim 0.94 \text{ g cm}^{-3}$  at  $P = 1 \text{ bar}$  and  $77 \text{ K}$  [32] and is named LDA. The HDA-to-LDA transition temperature increases with pressure, for example,  $T_{\text{HDA-LDA}} \sim 132 \text{ K}$  at  $P = 20 \text{ bar}$  (see Fig. 3 of Ref. [7]). The HDA-to-LDA transformation upon isobaric heating has been monitored using a range of techniques, such as volumetry [24], neutron and X-ray scattering [24,43–46], sound velocity and bulk-shear moduli measurements [39,47], thermal conductivity [39], and calorimetry experiments [48].

As shown in Fig. 3 of Ref. [7], a slight change in density is observed upon heating HDA at  $T < T_{\text{HDA-LDA}}$ . This is a continuous, irreversible relaxation process (annealing) during which a *family* of partially relaxed forms of HDA are produced [43–46]. This is followed by a sudden, jump-like change in density attributable to the polyamorphic transition to LDA. After HDA has transformed to LDA, further heating of LDA results in cubic ice ( $I_c$ ) at  $T \sim 152 \text{ K}$ , which transforms to ice  $I_h$  at  $T \sim 225 \text{ K}$ , and finally melts at higher temperatures. All these transformations (continuous relaxation of HDA, HDA-to-LDA, LDA-to-ice  $I_c$ , and ice  $I_c$ -to-ice  $I_h$ ) are clearly identified in the calorimetry experiments of Ref. [48]; see Fig. 4.

That water can exist in an amorphous solid state was known long time before the discoveries of HDA and LDA. In particular, amorphous ices were obtained by condensation of water vapor on a surface cooled below  $140 \text{ K}$  [49–51]

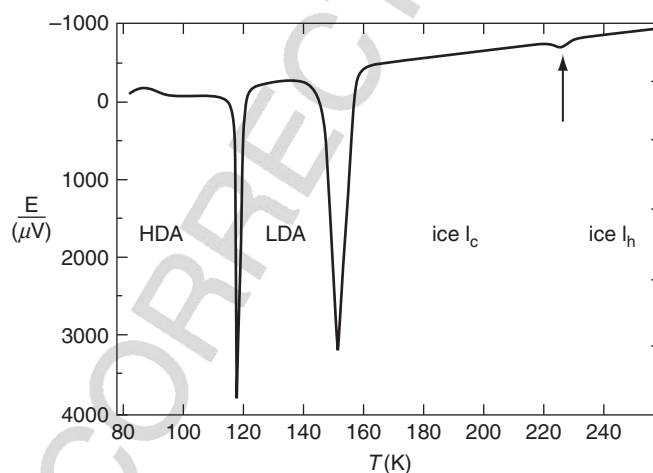


**Figure 4.** Voltage (microvolts) generated by the differential thermopile upon heating  $\sim 2.7 \text{ g}$  HDA sample at  $1 \text{ bar}$ . From left to right, exothermic peaks correspond to the HDA-to-LDA ( $\sim 117 \text{ K}$ ), LDA-to-ice  $I_c$  ( $\sim 152 \text{ K}$ ), and ice  $I_c$ -to-ice  $I_h$  ( $\sim 225 \text{ K}$ ; arrow) transition, respectively. Note the broad endotherm at  $T < 117 \text{ K}$ , which indicates continuous structural relaxation of HDA prior to the HDA-to-LDA transition. Adapted from Ref. [48].

(amorphous solid water, ASW), and by hyperquenching water droplets of several micrometer diameter at cooling rates of  $\sim 10^6 \text{K s}^{-1}$  (hyperquenched glassy water, HGW) [52–54], or by vitrifying liquid water films of  $< 1 \mu\text{m}$  thickness for cryoelectron microscopy [55]. Annealed ASW and HGW have both a density of  $\sim 0.94 \pm 0.01 \text{ g cm}^{-3}$  at 1 bar and  $T = 77\text{K}$  [32]. Since this is also the density of LDA at the same conditions [56] it is tempting to consider that ASW, HGW, and LDA are related. In Ref. [57], it is shown that indeed the radial distribution functions are identical at the resolution of the neutron diffraction experiment. Also, the glass transition temperatures are indistinguishable (see Section IX). However, it is shown in Ref. [58] that ASW, HGW, and LDA show different behavior upon annealing at 1 bar. Although the relationship between ASW, HGW, and LDA is not fully understood, it seems plausible that they can be considered as members, or substates, of a single family of low-density amorphous ices [59,60]. Different substates of LDA can not only be prepared by hyperquenching liquid droplets or water vapor deposition, but also by variation of the  $(P, T)$ -conditions in high-pressure experiments on pressure-amorphized ice [61].

#### IV. APPARENT FIRST-ORDER TRANSITION BETWEEN LOW- AND HIGH-DENSITY AMORPHOUS ICE

In Section 2, we discussed how compression of ice  $I_h$  at  $T = 77\text{K}$  produces HDA at  $P \sim 1 \text{ GPa}$ . A natural question follows, what is the product of compressing LDA at  $T = 77\text{K}$ ? Mishima et al. addressed this question; they found that compressing LDA at  $T = 77\text{K}$  results, surprisingly, in HDA [62].

The evolution of the piston displacement upon compressing the LDA sample is shown in Fig. 5. For comparison, the results obtained upon PIA of ice  $I_h$  are included. The LDA-to-HDA transformation occurs at  $P \sim 0.6 \text{ GPa}$ , as indicated by the sudden change in  $d(P)$ . This pressure is smaller than the pressure at which ice  $I_h$  transforms to HDA ( $\sim 1 \text{ GPa}$ ). Still, the LDA-to-HDA transition is at least as sharp as the ice  $I_h$ -to-HDA transition and, thus, it also resembles a first-order transition in its volume change. We note that the density of HDA at 1 bar and  $T = 77\text{K}$  is, within error bars, the same density of the HDA samples obtained from PIA of ice  $I_h$ ,  $\sim 1.17 \text{ g cm}^{-3}$ . Moreover, the X-ray diffraction patterns of HDA, obtained from ice  $I_h$  and LDA, are also very similar to each other [62]. Therefore, the HDA form obtained from LDA is apparently the same amorphous ice that results from PIA of  $I_h$  at  $T = 77\text{K}$  [24,62]. If the LDA-to-HDA transformation is indeed a true first-order transition, then one would expect to observe that HDA transforms back to LDA upon decompression. Otherwise, the LDA-to-HDA transformation could be interpreted as a simple relaxation effect of LDA. In this case, there would be a single amorphous phase of water (LDA) and HDA, instead of being a new amorphous phase different from LDA, would be a relaxed version of LDA [63]. Figure 5 shows

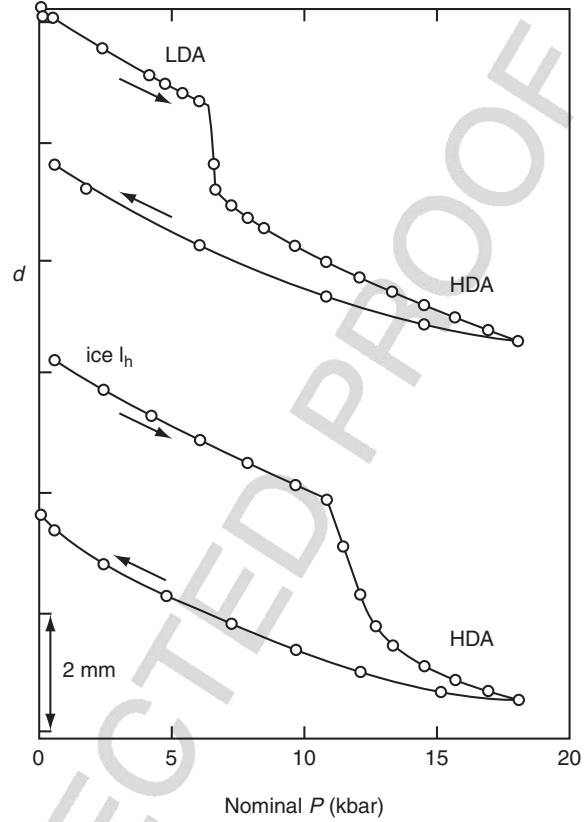


**Figure 5.** Piston displacement as function of pressure  $d(P)$  during the compression and subsequent decompression of LDA (top panel) and ice  $I_h$  (bottom panel) at  $T = 77\text{K}$ . LDA and Ice  $I_h$  transform to HDA at  $P \sim 0.6$  and  $\sim 1$  GPa, respectively. Sample pressures are slightly lower than nominal pressures. Adapted from Ref. [62].

that, similar to the case of ice  $I_h$ , the LDA-to-HDA transition is not reversible at  $T = 77\text{K}$ . However, experiments show that if the compression/decompression temperature is increased to  $T \sim 130\text{--}140\text{K}$  then HDA can be reconverted back to LDA upon decompression.

Figure 6 shows the volume of an LDA sample compressed to  $P \sim 1.2$  GPa, followed by decompression to 0 GPa [64]. During the compression/decompression process, the temperature of the sample increases slowly. The temperature in these experiments is in the range  $T \sim 130\text{--}140\text{K}$ . Since the compression/decompression temperature is close to LDA's glass transition temperature ( $T_g \sim 136\text{K}$ ) at which translational mobility increases (Section IX), it is easier for the amorphous ices to evolve from one phase to the other. At  $T \sim 130\text{--}140\text{K}$ , the LDA-to-HDA transition occurs at  $P \sim 0.3$  GPa and is even sharper than the corresponding transformation at  $T = 77\text{K}$  (trace a in Fig. 6). The sharpness of this transition suggests that there

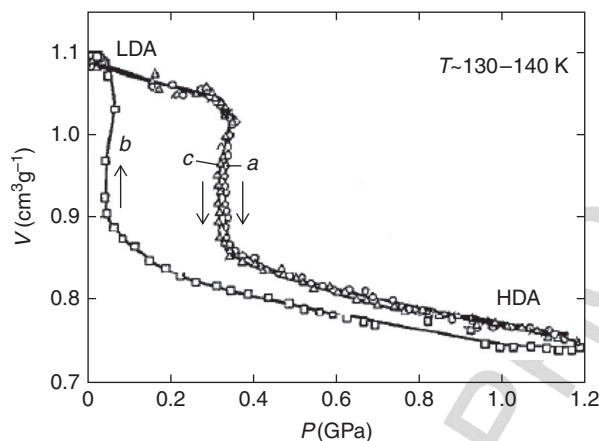


**Figure 6.** Volume as function of pressure during the (a) compression-induced LDA-to-HDA transition, (b) subsequent decompression-induced HDA-to-LDA transition, and (c) upon recompression of the LDA sample resulting from (b). The temperature increases slowly during the compression/decompression process and is in the range  $T \sim 130\text{--}140\text{ K}$ . Compression rate is  $\sim 0.6\text{ GPa min}^{-1}$ . Adapted from Ref. [64].

are no intermediate states between LDA and HDA. Upon decompression, HDA transforms back to LDA at  $\sim 0.05\text{ GPa}$  (trace b in Fig. 6); the transition being also remarkably sharp. The hysteresis in the reversible LDA–HDA transition is expected if this is considered to be a first-order transition. We note that the LDA–HDA transition is reproducible. For example, if the LDA sample, obtained upon decompression of HDA, is recompressed then HDA forms again at  $P \sim 0.3\text{ GPa}$  (trace c in Fig. 6). Recent isothermal experiments have shown that the transformation back to LDA is very sensitive to temperature changes and occurs only in a very narrow temperature interval between  $139\text{ K}$  and  $140\text{ K}$  ( $\pm 0.2\text{ K}$ ). The down-stroke transition occurs at  $\sim 0.06\text{ GPa}$  at  $140\text{ K}$  [65], and is shifted to  $\sim 0.02\text{ GPa}$  at  $139\text{ K}$  [66]. If done at  $136\text{ K}$ , negative pressures would be required for the HDA-to-LDA transformation to occur, and if done at  $142\text{ K}$  crystallization to ice IX interferes [66].

From the thermodynamics point of view, the possibility of having a first-order transition between amorphous solids is a very exciting and novel idea. It is not conclusive that the LDA-to-HDA transformation is, indeed, a first-order transition. For this to be the case, it would be sufficient to observe the nucleation of HDA from LDA, growth of the HDA phase as the pressure increases (coexisting with LDA), until all the sample becomes HDA. Similarly, one should be able to observe the nucleation of LDA from HDA, growth of the LDA phase as pressure decreases, until all the sample becomes LDA. Although these nucleation processes have not



**Figure 7.** Amorphous ice sample (1.5 mL) made by decompression of VHDA (see Section VII) at 140K to 0.07 GPa with a rate of  $13 \text{ MPa min}^{-1}$  and then quench-recovered to 77K and 1 bar (top image). After removal from the piston cylinder apparatus, the sample easily broke into two pieces; the two separated pieces were placed on a copper block kept at 77K (second from top). The bottom two images show the two pieces in the course of heating to 250K at 1 bar.

been observed in pure amorphous ice, photographs of LDA and HDA coexisting in a single sample have been reported [67,68]. In Ref. [67] HDA and LDA are observed in the same sample, separated by a clear boundary region in thin film samples in the interior of a diamond anvil cell (*in situ*). In Ref. [68] the same phenomenology was observed in much larger bulk samples on the downstroke (see curve b in Fig. 6). A sample quench-recovered from 0.07 GPa and 140K to 77K and 1 bar after decompression is shown in Fig. 7. The *ex situ* characterization by Winkel et al. shows a spatially heterogeneous sample. The top image in Fig. 7 shows the sample after removal from the piston cylinder apparatus. This sample consists of two pieces, well separated by a visible boundary. The area of rupture is visible in the top image as a white line (fissure) close to the middle of the sample cylinder. The second image from top shows the sample after having pulled the two pieces apart by tweezers. Upon heating at ambient pressure it is clearly evident that the two pieces do not behave alike. Whereas one piece (left in Fig. 7) transforms to a lower density phase, the other piece (right in Fig. 7) does not transform to a lower density phase (bottom two images in Fig. 7). That is, the original cylindrical sample is a macroscopically segregated mixture of

a high-density part and a low-density part, and easily breaks where low-density and high-density parts abut [68]. In addition to the visual experiment depicted in Fig. 7, also X-ray, Raman, and calorimetric measurements show that the two pieces are distinct phases, namely HDA (left in Fig. 7) and LDA (right in Fig. 7) [69]. X-ray diffraction experiments on sample chips picked from the site of fracture (in the vicinity of the fissure seen in the top image in Fig. 7) show patterns, which can be explained by the superposition of LDA and HDA [68]. By contrast, sample chips taken a few millimeters away from the site of fracture produce X-ray diffraction patterns corresponding either to LDA or to HDA, that is, pure phases. *When repeating the experiment several times the LDA phase was observed in some cases to appear on the “left” side and in other experiments on the “right” side. In one instance the sample even appeared as a sandwich of alternately LDA and HDA [69]. That is, LDA grows at random either from the bottom up or from the top down within the high-density sample, and ends up either on the “left” or on the “right”* <sup>A</sup>

The results of Ref. [67] and Ref. [68] strongly suggest that the HDA–LDA transition is indeed a first-order transition, and that an interface between LDA and HDA is obtained. With time the LDA grows at the expense of the HDA matrix upon decompression. This view is also supported by recent neutron diffraction experiments obtained for the reverse transition from LDA to HDA upon compression. In Ref. [70], it is shown that neutron diffraction patterns of samples obtained upon compression of LDA show a “double-peaked” halo maximum, one peak being characteristic of LDA and the other peak being characteristic of HDA. Also, Raman spectra obtained under pressure were interpreted in favor of a mixture of HDA and LDA [71].

## V. AN INTERPRETATION OF AMORPHOUS ICE PHENOMENOLOGY FROM COMPUTER SIMULATIONS

The  $T$ – $P$  phase diagram of ice together with the boundaries between the ice, LDA, and HDA regions is indicated in Fig. 8 (left panel). The amorphous solid phases exist only below  $T_X(P) \sim 150$ – $160$ K (see also Fig. 1). Above this temperature, amorphous ice crystallizes. Few years after the discovery of HDA and LDA, scientists used computer simulations to study amorphous ice [72,73]. ~~While crystallization is unavoidable above  $T_X(P)$  in experiments, computer simulations are limited by the accessible timescales. Computer simulation timescales are usually short enough that crystallization is not observed, allowing for the study of the relationship between the liquid and the glass state. This also implies that the glasses obtained in simulations are characterized by cooling/heating and compression/decompression rates that are  $\sim 8$ – $9$  orders of magnitude shorter than the corresponding rates that are typically used in experiments. Nonetheless, many of~~

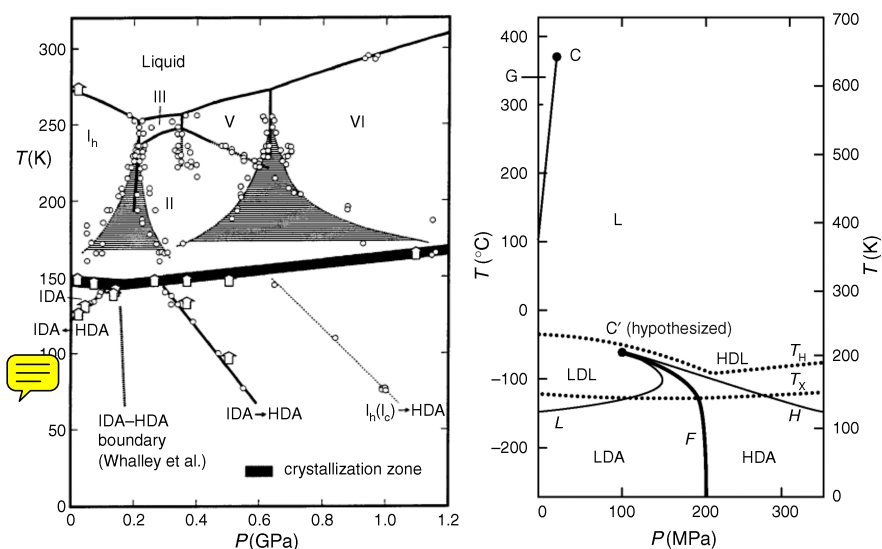


**Figure 8.** Left panel: phase diagram of ice and transition lines corresponding to the ice  $I_h$ -to-HDA, LDA-to-HDA, and HDA-to-LDA transformations as obtained in experiments. The thick black line is the crystallization temperature  $T_X(P)$  above which amorphous ice crystallizes. For pressure-induced transitions, a large hysteresis is found both for the LDA-HDA and crystal-crystal transitions. Open circles indicate pressure-induced transitions; temperature-induced transitions are indicated by arrows. The ice  $I_h$ -to-HDA transition line as well as the estimated LDA-HDA coexistence line from Ref. [74] is included. Adapted from Ref. [64]. Right panel: phase diagram proposed to explain water liquid anomalies and the existence of LDA and HDA. A first-order transition line (F) extends above the  $T_X(P)$  line and ends in a second critical point ( $C'$ ). The second critical point is located in the supercooled region, below the homogeneous nucleation temperature  $T_H(P)$ . LDL and HDL are the liquid phases associated with LDA and HDA, respectively. The LDA-to-HDA and HDA-to-LDA spinodal lines are indicated by H and L, respectively. C is the liquid-vapor critical point and is located at the end of the liquid-vapor first-order transition line (G). From Ref. [60].

the transformations observed in experiments, such as the ice  $I_h$ -HDA and LDA-HDA transitions, are reproduced qualitatively in simulations.

In 1992, Poole et al. performed classical molecular dynamics (MD) simulations of water using the ST2 model, both in the liquid and glass state [75]. Their simulations lead to a novel interpretation to explain both glassy water polyamorphism and liquid water anomalous properties. In their view (see Fig. 8, right panel), LDA and HDA are separated by a first-order transition line at very low temperature (as suggested previously in Ref. [62]). This line continues above the glass transition temperature into the liquid phase and ends in a novel second CP ( $C'$ ); the first CP (C), being the liquid-gas CP. This hypothesized second CP was estimated to be located at  $P_c \sim 220$  K,  $T_c \sim 0.1$  GPa, and  $\rho_c \sim 1$  g cm $^{-3}$  [76]. Since the second CP is

located below the homogeneous nucleation temperature, below which liquid water crystallizes, and above  $T_X(P)$ , above which glassy water crystallizes, the second CP is difficult to detect experimentally due to crystallization. The short computer simulation timescales, short enough that crystallization is avoided, are the reason that one could observe this CP in simulations. Included in Fig. 8, right panel, are the LDA-to-HDA and HDA-to-LDA spinodal lines. In analogy to liquid–vapor first-order transitions [77], the LDA-to-HDA spinodal line represents the  $T$ – $P$  values above which LDA becomes unstable relative to HDA. The region limited by this spinodal line (H) and the coexistence line (F) corresponds to the  $P$ – $T$  values where LDA is “metastable” relative to HDA. Although at these  $P$ – $T$  values LDA has a higher free energy than that of HDA, no thermodynamic condition of stability is violated. Similarly, the HDA-to-LDA spinodal line indicates the region of the  $P$ – $T$  plane above which HDA becomes unstable relative to LDA; the region limited by this spinodal line (L) and the coexistence line (F) corresponds to the  $P$ – $T$  values where HDA is “metastable” relative to LDA. The well-separated spinodal lines would be the reason of the hysteresis observed in the LDA–HDA transitions upon compression/decompression (Fig. 6). Upon compression, LDA transforms to HDA at the LDA-to-HDA spinodal line, while upon decompression, HDA transforms to LDA at lower pressure corresponding to the HDA-to-LDA spinodal line.

There are a few experiments supporting that a second CP may indeed exist in water [60,76]. Up to date, the existence of a second CP in water has not been confirmed. We note that the second CP hypothesis is not the only explanation of water polyamorphism; theoretical interpretations of water polyamorphism that do not consider the presence of a second CP in supercooled water have also been proposed (see, e.g., Ref. [2]).

## VI. DIFFERENT STATES OF RELAXATION IN HDA

We have alluded to two methods to produce HDA so far, namely PIA of ice  $I_h$  at 77K (Section II) and compression of LDA at  $\sim 77$ –140K (Section IV). These states barely differ in terms of structure as judged by diffraction experiments. However, they differ significantly in terms of their state of relaxation and thermal stability at ambient pressure. For this reason, Nelmes et al. have introduced the terms “unannealed HDA” (uHDA) and “expanded HDA” (eHDA) to identify HDA samples [42]. The former refers to the highly unrelaxed (strained) form of HDA obtained by PIA of ice  $I_h$  at 77K, whereas the latter refers to relaxed forms of HDA obtained at higher temperature. Specifically, Nelmes et al. have noted a small shift in the position of the broad halo peak to lower d-spacings of X-ray diffraction patterns of uHDA samples that were heated isobarically to 125–130K at  $P < 0.2$  GPa. The change in d-spacing was assigned to an expansion of the sample and hence the name of eHDA given to these amorphous ices [42]. Cryoflotation experiments

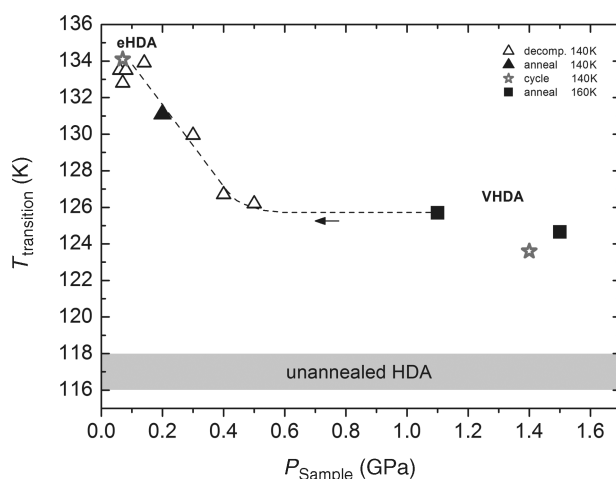


**Figure 9.** Thermal stability of various amorphous ices at ambient pressure. Samples were quench-recovered at 77K and 1 bar, and heated at a rate of  $10\text{K min}^{-1}$  using a differential scanning calorimeter.  $T_{\text{transition}}$  is the temperature at which the samples transform to LDA. Closed squares: VHDA samples (Section VII) obtained by isobaric heating uHDA at high pressure ( $P_{\text{sample}} = 1.1$  and  $1.5$  GPa) to 160K. Open triangles: HDA samples decompressed at 140K to  $P = P_{\text{sample}}$  and then quench-recovered from the selected pressure. Closed triangle: HDA sample heated to 140K at 0.2 GPa. Stars: decompression cycle between eHDA and VHDA at 140K (see Fig. 10). Unannealed HDA is prepared at 77K by pressure-induced amorphization of ice  $I_{\text{h}}$  (see Section II). The data are taken from Refs [21,68]. Symbol sizes represent error bars of  $\pm 0.5\text{K}$ .

by Loerting et al. confirm that eHDA indeed has a density that is lower than the density of uHDA by  $0.02\text{ g cm}^{-3}$  [32]. Most notably, the resistance to transform to LDA and hence the thermal stability at ambient pressure increases significantly for more relaxed samples. Figure 9 shows an analysis of the thermal stability of various HDA samples as judged from DSC experiments at 1 bar and  $10\text{K min}^{-1}$  [69]. uHDA (gray bar in Fig. 9) transforms at  $117 \pm 1\text{K}$  to LDA, ~~independently of the pressure considered.~~ Instead, eHDA prepared by annealing uHDA to 140K at 0.2 GPa and recovered at 1 bar and 77K (as proposed by Nelmes et al. [42]) transforms to LDA at 131K (black filled triangle in Fig. 9). An even higher stability can be achieved by ~~the route of decompression of HDA samples~~ at 140K just prior to the transformation to LDA at  $p < 0.1$  GPa (i.e., for a HDA sample close to the state shown in Fig. 7). Such samples, recovered at 1 bar and 77K, transform to LDA at 134K, that is, 17K higher than uHDA. Higher thermal stability at ambient pressure indicates a higher degree of relaxation, and so the sample transforming at 134K to LDA corresponds to the most relaxed form of HDA known at ambient pressure so far [68].

## VII. VERY HIGH-DENSITY AMORPHOUS ICE

In Ref. [37], Mishima briefly stated that HDA formed by PIA of ice  $I_h$  at temperatures in the range  $\sim 120$ – $150$  K differs from HDA obtained by PIA at  $T = 77$  K. In particular, he observed that the thermal stability of these samples, recovered at 1 bar, increases as the compression/decompression temperature increases; the HDA  $\rightarrow$  LDA transformation temperatures upon isobaric heating at 1 bar are  $T_{\text{HDA-LDA}} \sim 117$  K and  $T_{\text{HDA-LDA}} \sim 125$  K for compression/decompression temperatures  $T \sim 77$  K and  $T \sim 145$  K, respectively. Structural differences in the HDA samples obtained at different compression temperatures are also present and are evidenced, for example, by a shift in the broad halo peak of the corresponding X-ray diffraction patterns.

The changes observed in HDA samples obtained at different compression temperatures are also found in HDA samples that are produced by PIA of ice  $I_h$  at  $T = 77$  K (i.e., uHDA) and then heated at constant pressure (i.e., *annealed*) at  $P > 1$  GPa up to  $T > 130$  K [37]. This suggests that the same distinct HDA state is formed upon (i) annealing uHDA at high pressure and (ii) PIA of ice  $I_h$  at high temperature. In 2001, Loerting et al. investigated the changes in HDA occurring upon annealing samples at  $P > 1$  GPa using dilatometry experiments [78]. They determined that the density of the resulting “annealed” HDA (obtained at  $T > 130$  K and  $P > 1.1$  GPa), recovered at 77 K and 1 bar, is  $1.25 \text{ g cm}^{-3}$ . This amorphous solid is  $\sim 9\%$  denser than the recovered “unannealed” HDA, obtained at  $T = 77$  K by PIA of ice  $I_h$  ( $\sim 1.17 \text{ g cm}^{-3}$ ). Moreover, in Figure 7.1D of Ref. [78], it is reported that the annealed HDA can be transformed back to an unannealed HDA-like state by heating it at constant volume to  $\sim 140$  K (accompanied with a pressure increase from 0.02 GPa, at 80 K, to 0.14 GPa, at  $\sim 140$  K). The difference in density at 1 bar (and thus molecular structure) of the annealed and unannealed HDA forms, as well as the possibility of switching back and forth between these HDA states, prompted the need for giving a name to HDA *obtained at  $P > 0.8$  GPa and  $T > 130$  K*. This amorphous ice has been named VHDA [78].

Figure 9 shows calorimetry data of VHDA prepared by annealing uHDA at 1.1 GPa to 160 K (filled square at 1.1 GPa) [68]. In agreement with the data by Mishima, VHDA transforms to LDA at  $125 \pm 1$  K and ambient pressure [37]. Empty triangles and dashed line in Fig. 9 show the transition temperature ( $T_{\text{transition}}$ ) to LDA for samples of VHDA that are decompressed at  $T = 140$  K to  $P = P_{\text{sample}}$  and then recovered at 77 K and 1 bar.  $T_{\text{transition}}$  remains practically constant for decompression to  $P \sim 0.4$  GPa, whereas decompression to  $P < 0.4$  GPa at 140 K produces samples of increasing thermal stability. The highest thermal stability of an HDA sample at ambient pressure is obtained when decompressing to 0.07 GPa (see Fig. 7 and Section VI).

The discovery of VHDA implies that scenarios involving a single first-order-like transition between LDA and HDA (see Section V) may need to be modified since

the possibility of a second first-order-like transition between HDA and VHDA, which can end in a third critical point, has to be considered. The relation between LDA, HDA, and VHDA, and the nature of the corresponding transformations have been explored on the grounds of compression experiments of LDA and decompression experiments of VHDA in the temperature range 125–140K [65,66,79]. These experiments show that all three amorphous ices are connected and that they can be reversibly obtained in a single isothermal compression or decompression experiment via the sequence  $\text{LDA} \rightleftharpoons \text{HDA} \rightleftharpoons \text{VHDA}$ . While these experiments indicate a sudden jump in density and a possible discontinuity between LDA and HDA upon changing pressure (see also Fig. 6), the nature of the transformation between HDA and VHDA is continuous. Yet, VHDA transforms to HDA in a rather narrow pressure interval [65,68] upon decompression and HDA transforms to VHDA in a rather narrow pressure interval upon compression [79]. Also, there is a jump-like change from a HDA diffraction pattern to an LDA diffraction pattern upon decompressing HDA at 140K to  $P \sim 0.08\text{--}0.06$  GPa, whereas the diffraction pattern of VHDA evolves slowly to the HDA diffraction pattern at  $P \sim 0.08\text{--}0.40$  GPa [65]. Also the calorimetry data shown in Fig. 9 (dashed line) shows that VHDA transforms to HDA only at  $P \sim 0.08\text{--}0.40$  GPa, but not at  $P > 0.40$  GPa.

The possibility of transforming HDA and VHDA reversibly into each other is illustrated in Fig. 10. Figure 10a shows the piston displacement upon decompressing VHDA at 140K to 0.07 GPa (from point 1 to point 2), recompressing to 1.4 GPa (from point 2 to point 3), and a final decompression to 0.07 GPa (point 4). Powder X-ray diffractograms of samples quench-recovered from points 1 and 3 (Fig. 10b, top two diffractograms) are practically indistinguishable and correspond to VHDA. Also powder X-ray diffractograms of samples quench-recovered from points 2 and 4 are practically indistinguishable (Fig. 10b, bottom two diffractograms), but correspond to eHDA. The halo maximum is shifted by  $2\Theta \sim 3^\circ$  between the two sets of diffractogram (dashed lines in Fig. 10b). The thermal stability at ambient pressure is indicated in Fig. 9 at point 1 by the filled square at 1.1 GPa, at points 2 and 4 by the star at 0.07 GPa, and at point 3 by the star at 1.4 GPa. Clearly, the transition temperature to LDA at ambient pressure ( $T_{\text{transition}}$  in Fig. 9) can also be shifted back and forth by repeatedly compressing and decompressing at 140K. The reversible nature and the finite and narrow pressure interval suggest that VHDA is indeed a structural state different from HDA, even though the HDA–VHDA transition does not have the character of a first-order transition.

The interpretation that VHDA is still a distinct amorphous material and should be considered the third amorphous ice “phase” is supported by the data shown in Fig. 11. Figure 11 shows the density of amorphous ices obtained by compressing recovered HDA at  $T = 77\text{K}$  to different pressures, followed by annealing to temperatures just below the corresponding crystallization temperature. The data can be fitted quite nicely by two straight lines. The first straight line in the pressure range 0.3–0.8 GPa extrapolates to a density of roughly  $1.15 \text{ g cm}^{-3}$  at 1 bar,

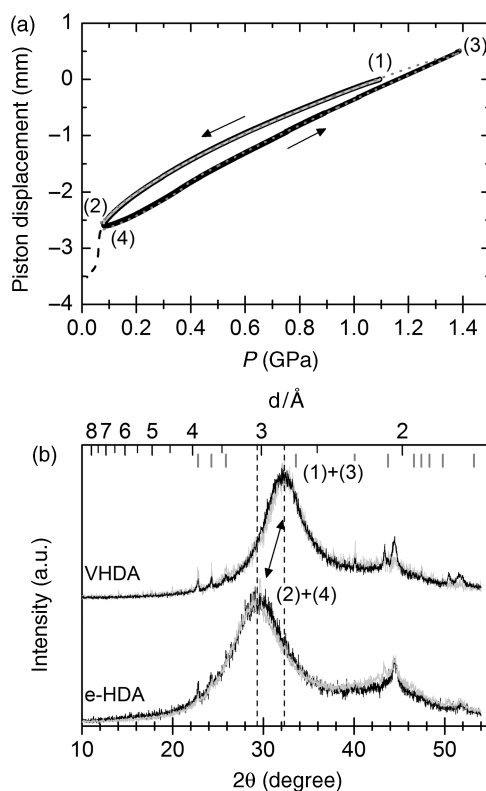


**Figure 10.** (a) Isothermal decompression/compression cycles between VHDA and eHDA at 140K and a rate of  $20 \text{ MPa min}^{-1}$ . VHDA at point (1) is decompressed to point (2), recompressed to point (3), and finally decompressed to point (4). (b) X-ray diffractograms after quench-recovery to 77K and 1 atm from the (4) points indicated in (a). Diffractograms (1) and (3) are  $y$ -shifted against diffractograms (2) and (4) for clarity. Samples (1) and (3) correspond to VHDA, while samples (2) and (4) correspond to eHDA.

which corresponds to the density of uHDA [24,78]. The second straight line in the pressure range 0.8–1.9 GPa extrapolates to a density of  $1.25 \text{ g cm}^{-3}$  at 1 bar, which corresponds to the density of VHDA [78]. Thus, the data suggests that HDA states are observed close to the crystallization temperature at  $P < 0.8 \text{ GPa}$ , whereas VHDA states are observed at  $P > 0.8 \text{ GPa}$ . The slopes of the two fitting lines play the role of compressibilities of HDA (or, more precisely, eHDA) and VHDA just below the crystallization line.

The finding that the VHDA-to-HDA transformation is continuous [65], as opposite to the pressure-induced, apparently discontinuous LDA–HDA transformations, has implications for our understanding of the metastable phase diagram of amorphous supercooled and glassy water. It seems counterintuitive that a continuous amorphous–amorphous transition at  $\sim 140\text{K}$  changes character into a discontinuous liquid–liquid transition when performed above  $T_g$ . On the other hand, it seems quite possible that a first-order-like amorphous–amorphous transition develops into a first-order liquid–liquid transition when performed above  $T_g$ . Since first-order

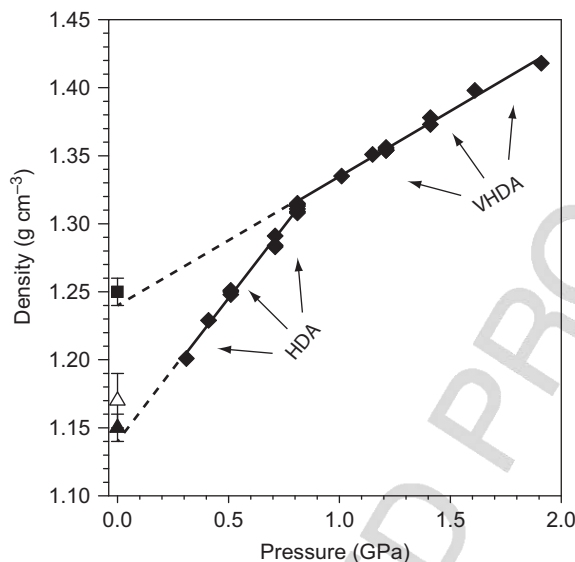


**Figure 11.** Densities of amorphous ice samples as a function of pressure just below the crystallization temperature, which increases from 144K at 0.3 GPa to 183K at 1.9 GPa. The data suggests there are two linear pressure ranges, corresponding to two distinct amorphous ices. The densities of these amorphous solids correspond to the densities of HDA in the range from 0.3 GPa to 0.8 GPa and to the densities of VHDA in the range from 0.8 GPa to 1.9 GPa. The linear region corresponding to LDA cannot be seen on this scale since its density is  $\sim 0.92\text{--}0.94\text{ GPa g cm}^{-3}$  in the pressure range up to 0.2 GPa. The densities of unannealed HDA (open triangle: measurement by Mishima [24]; filled triangle: measurement by Loerting et al. [78]) and VHDA (filled square: measurement by Loerting et al. [78]) at 77K are shown at 0 GPa. Adapted from Ref. [22].

transitions between two isotropic phases, such as gas–liquid or liquid–liquid transitions, can generally end in a critical point, the experimental finding of a continuous HDA–VHDA, but discontinuous HDA–LDA transition, does not rule out the existence of a second critical point (between a low-density liquid (LDL) and a high-density liquid (HDL)), but strongly disfavors a third critical point (between HDL and a very high-density liquid (VHDL)). Future experiments conducted at higher compression/decompression temperatures, say  $\sim 180\text{K}$ , may conclusively demonstrate whether a discontinuous VHDA-to-HDA transition may nevertheless exist. Above 180K, crystallization rates are so high that it is almost impossible to study the VHDA-to-HDA transition in experiments.

We note that other interpretations for the HDA–VHDA transformation are, in principle, possible. For example, Andersson et al. [80–84] (see Section X, Figure 15) studied the glass transition of VHDA at 1 GPa and find evidence that water should be liquid at 1 GPa and  $T > 140\text{K}$ . If this finding is confirmed, then

a more appropriate term for VHDA at  $T > 140\text{K}$  would be VHDL. In particular, this would give rise to the possibility that the continuous transition reported by Winkel et al. at 140K [65,68,69] may indeed be a supercritical transition and that a critical point may be located at lower temperature, for example, 125K at 0.8 GPa. We currently regard samples at 125K and 0.8 GPa to be deep in the glassy region, but the experiments by Andersson et al. [80–84] suggest that this may not be the case. A scenario of a low-lying VHDL–HDL critical point is clearly speculation on the basis of the current experiments, and an assessment of the merits of such a scenario requires systematic *in situ* experiments investigating whether or not critical phenomena are observable and whether or not VHDA shows liquid-like properties at  $T > 140\text{K}$ .

### VIII. MOLECULAR STRUCTURE OF AMORPHOUS ICES

Despite the higher density of VHDA, relative to HDA, Raman spectroscopy [78] and isotope-substitution neutron diffraction [85] studies indicate that the average O–O distances of hydrogen-bonded molecules is longer in VHDA than in HDA, namely 2.85 Å compared to 2.82 Å. In LDA the O–O distance is even shorter than in HDA, namely 2.77 Å [78,86]. This apparent paradox of higher density, but longer hydrogen bonds, can be resolved by looking at the local tetrahedral structure of water, as shown by the Walrafen pentamer in Fig. 12d. The Walrafen pentamer represents approximately the local structure in LDA, where a central molecule is surrounded by four nearest molecules in a tetrahedral-like arrangement; these four neighbors constituting the “first shell” of the central molecule. In the case of LDA, there is an empty shell separating the first and second neighbor shells. It has been shown that in HDA and VHDA additional molecules locate in the first interstitial shell, in the region close to the tetrahedron faces of the Walrafen pentamer structure, thereby disturbing the Walrafen pentamer arrangement [85]. Specifically, in case of HDA, roughly one interstitial site is occupied by a water molecule, whereas in VHDA two such interstitial sites are occupied. uHDA and eHDA show the same structural motif and only small differences in their radial distribution function [21]. Each time a molecule moves in, from the second coordination shell of water molecules to the interstitial shell, water molecules in the Walrafen pentamer are forced to move slightly apart, increasing the O–O distance between the central molecule and its first nearest neighbors, while the density of the glass increases. Therefore, the third structural state of amorphous ice (VHDA) shows a structural motif that is as different from HDA as the motif in HDA is from LDA. Both differ by one full interstitial water molecule, resulting in a local coordination number decrease from 6 in VHDA, to 5 in HDA, and 4 in LDA. This picture is also observed in computer simulations [87,88]. The refined experimental O–O, OH-, and HH-radial distribution functions [56,85], which

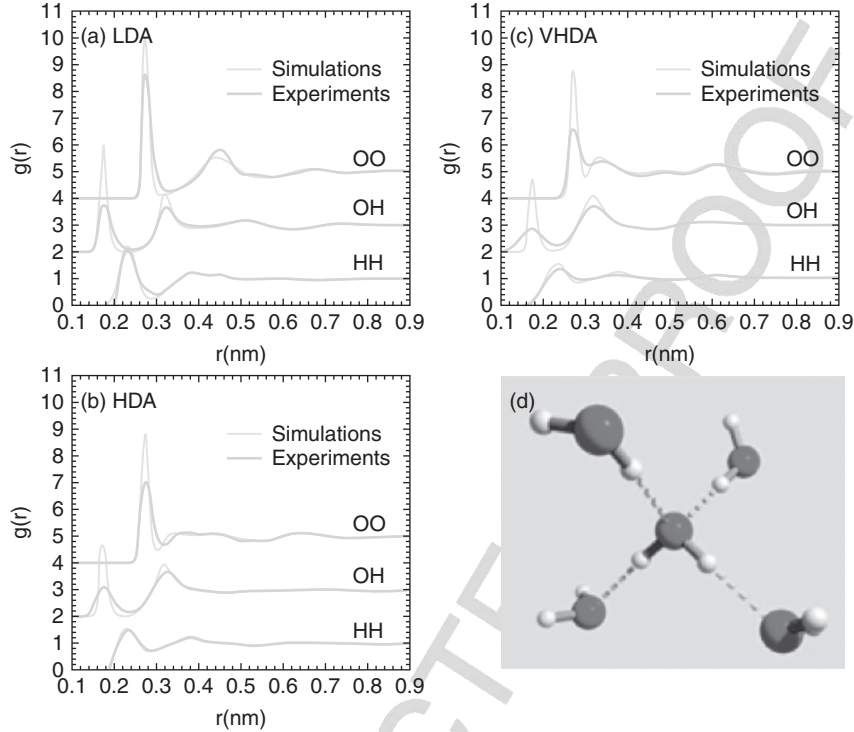


**Figure 12.** Radial distribution functions of (a) LDA, (b) HDA, and (c) VHDA as compared between simulations [87] and experiment [56,85]. (d) The Walrafen pentamer is the basic structural motif common to all amorphous ices. Adapted from Ref. [7].

have yielded this molecular level picture of amorphous ices at the short range, are shown along with simulation data in Fig. 12. It is evident that the same structural trends are reflected in the simulations [87].

### IX. VHDA IN COMPUTER SIMULATIONS

Computer simulation studies of the relationship between HDA and VHDA were published soon after the discovery of VHDA [89,90]. In Refs [89,90], the HDA-to-VHDA transformation was reproduced in MD simulations using the TIP4P and SPC/E water models. In these works, the same annealing procedure followed in experiments at high pressure [78] was used. These results from computer simulations are in quantitative agreement with experiments. For example, the evolution of density with temperature upon heating uHDA configurations at  $P = 1.38$  GPa, from the simulations using the SPC/E model, is shown in Fig. 13b [90].

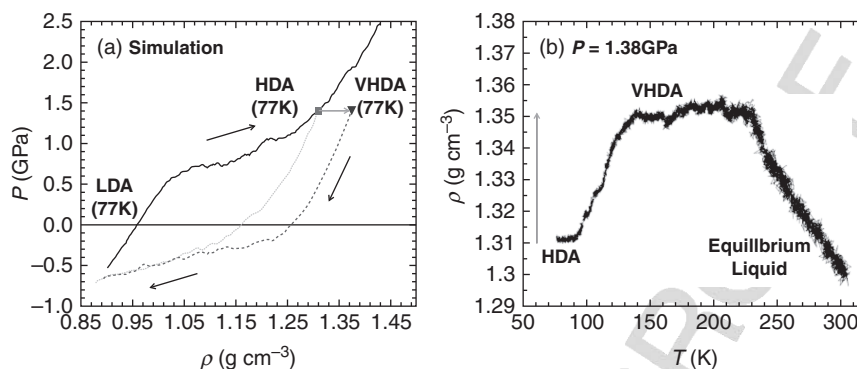


**Figure 13.** (a) Pressure versus density during the (i) LDA-to-HDA transition (solid line), (ii) decompression of HDA at  $T = 77$  K (dotted line), and (iii) decompression of VHDA at  $T = 77$  K (dashed line). The gray arrow indicates the density change in HDA upon isobaric heating at  $P = 1.38$  GPa from  $T = 77$  K (square) to 165 K, followed by cooling back to  $T = 77$  K (triangle). (b) Evolution of density upon annealing HDA at  $P = 1.38$  GPa. From Ref. [87].

Figure 13b is remarkably similar to the experimental data shown in Figure 7.1D of Ref. [78]. As in the experimental case, the HDA configurations used to produce VHDA upon annealing (Fig. 13b) were obtained by compressing LDA at  $T = 77$  K [90]. The pressure as function of density during the simulated LDA–HDA transformations is shown in Fig. 13a and are also in agreement with experiments (see Fig. 5). There are a large number of computer simulations using different water models that reproduce the pressure-induced LDA–HDA transformations; see for example, Ref. [7]. We note that the computer simulations of Refs. [89,90] also reproduced qualitatively the structural changes between LDA, HDA, and VHDA (Fig. 12), as well as the densities of HDA and VHDA at high pressure and after decompression at 1 bar [87,88] (Fig. 11).

In Refs [89,90], the density of HDA configurations annealed at different pressures was also explored. The resulting density versus annealing pressure plot shows a crossover similar to that observed in Fig. 11 (see Figure 16 in [7]). The main finding of Refs [89,90] is that similar annealing effects to those observed at  $P > 1$  GPa, corresponding to the HDA-to-VHDA transition, can be observed at intermediate pressures ( $\sim 0.15 < P < 1$  GPa). This observation led to the interpretation that the HDA-to-VHDA transition, resulting from annealing, is a general relaxation effect due to increasing the temperature at constant pressure. The conclusion from Refs [89,90] is, therefore, that VHDA, although structurally distinct from HDA, can be viewed as a “relaxed” version of HDA. This is the view originally proposed by Mishima [37,91], that is, VHDA and HDA both correspond to states in the same megabasin of the system configuration space [92].

MD simulation studies where LDA is compressed at  $T = 77\text{K}$  have been performed using different models, such as the SPC/E, TIP4P, and ST2 models [75,87,93]. The evolution of density with pressure obtained in these works shows a single density step, corresponding to the LDA-to-HDA transition (see, for example, Fig. 13a). However, a second density step, corresponding to the HDA-to-VHDA transition, is not observed in these works. It is not clear whether such a second density step can be reproduced with slower compression rates.

In a recent work, computer simulations using replica exchange MD, a MD technique that enhances sampling by approximately two orders of magnitude, provide an alternative view of the relationship of HDA and VHDA [94]. In this work, liquid water was studied at very low temperature,  $T \geq 150\text{K}$ , using the TIP4P-Ew model. The low- $T$  isotherms in the  $P$ - $\rho$  plane show two density steps. Thus, the results of Ref. [94] support the view that two-phase transitions occur in amorphous ice, the LDA-HDA and HDA-VHDA transition [95,96]. The results of Ref. [94] seem to indicate that the HDA-to-VHDA transition is a first-order transition. However, as the authors indicate, it is also possible that such a transition is of higher order [94].

The results from computer simulations and the corresponding interpretations should be taken with caution since some results, especially in the low-temperature domain, can be model-dependent and sensitive to technical simulation details. In Refs [95,96], the phase diagram of water using the SPC/E, TIP4P, and ST2 models was studied using Monte Carlo (MC) simulations in the Gibbs ensemble and in the density fluctuation-restricted NPT ensemble. MC simulations in the density fluctuation-restricted NPT ensemble [95,96] indicate that, depending on the technique used to treat the long-range electrostatic interactions, these models can present different multiple liquid-liquid first-order transitions ending in different CPs. In particular, the results obtained with the ST2 model were used as support of the view that VHDA is a new amorphous ice, different from HDA. In Refs [95,96], it is proposed that, similar to the case of LDA and HDA, VHDA and HDA are separated by a first-order transition line, that ends in a third CP. The same conclusion is supported by MC simulations in the Gibbs ensemble using a polarizable water model [97]. Multiple first-order transitions have been observed in computer simulations of liquids other than water (see, e.g., [98,99]). However, we note that the existence of a third CP, and a first-order transition between HDA and VHDA, is difficult to maintain after the experiments of Ref [65], which show a continuous VHDA-to-HDA transition. Moreover, this view is not supported by a recent work [100] where histogram reweighting MC simulations in the grand-canonical ensemble were performed using the ST2 model. This technique does not restrict density fluctuations, as is the case of the simulations of Refs [95,96]. Their results indicate that, contrary to the findings of Refs [95,96], no third CP at  $T > 217\text{K}$  exist in ST2 water. Only the second CP found originally in Ref. [75] was observed.

### X. THE GLASS-TO-LIQUID TRANSITION

The most commonly employed method to study the glass-to-liquid transition is calorimetry, in particular DSC. Whereas below  $T_g$  molecular translational and rotational mobility are frozen-in, these degrees of freedom become unfrozen at temperatures in the vicinity of  $T_g$ . Therefore, as the temperature of the glass is raised, a sudden increase in the isothermal heat capacity,  $C_p(T)$ , is observed at  $T \sim T_g$ . This sudden increase in  $C_p(T)$  results in an excess specific heat  $\Delta C_p$  between  $C_p(T)$  in the liquid and glassy state.

Figure 14 shows the heat exchange (proportional to  $C_p(T)$ ) during DSC experiments using HGW, ASW, and LDA samples at  $P = 1$  bar. In the case of HGW, the glass transition was found to take place at  $T_g \sim 136 \pm 2$  K. The corresponding increase in  $C_p(T)$ , indicated by the small peak at  $T \sim 150$  K in Fig. 14, is  $\Delta C_p \sim 1.6 \text{ JK}^{-1} \text{ mol}^{-1}$  [101]. This value of  $\Delta C_p$  was later shown to include an overshoot effect; without this overshoot  $\Delta C_p \sim 0.7 \text{ JK}^{-1} \text{ mol}^{-1}$  [54,104]. In Fig. 14, the glass-to-liquid transition at  $T_g$  is immediately followed by crystallization to cubic ice; the onset of crystallization occurs at  $T_x$ . The value of  $\Delta C_p$  measured in the case of HGW is one of the smallest values ever measured [101]. The small magnitude of  $\Delta C_p$  has resulted in a vivid discussion regarding whether this is indeed a glass-to-liquid transition. At present, it is accepted by many that  $T_g \sim 136$  K for HGW at 1 bar [2,54,104–108], and that the deeply supercooled liquid in the window between 136 K and 150 K shows a temperature dependence of structural relaxation time and viscosity different from ambient water (corresponding to a “strong” vs. “fragile” transition in liquid water, using the liquid classification introduced by Angell [109,110]). Other interpretations regarding the small

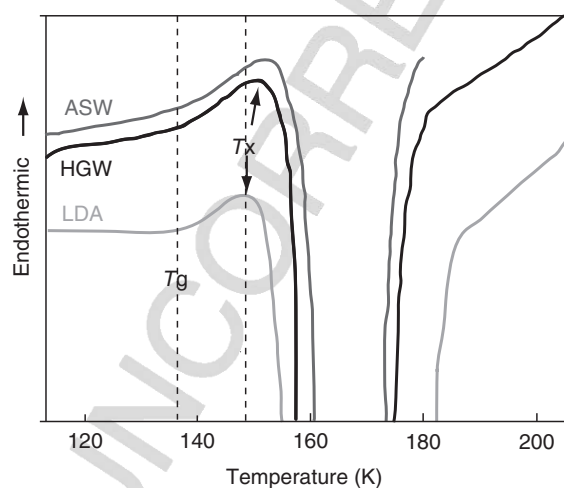


**Figure 14.** DSC scans of ASW, HGW, and LDA. All traces are recorded at  $30 \text{ K min}^{-1}$  after prior annealing at 127–130 K for at least 90 min. Vertical dashed lines mark the glass transition temperature  $T_g \approx 136$  K, for all three samples, and the crystallization temperature  $T_x \approx 148$  K, for the case of LDA. In between these vertical lines the sample is in an ultraviscous, deeply supercooled liquid state. Adapted from Refs [101–103].

$\Delta C_p$  step at  $\sim 136\text{K}$  have been introduced in the literature. In particular, the small  $\Delta C_p$  step has been associated with a “conformational” glass transition [111] and a “shadow” glass transition [112]. The “conformational” glass transition involves the unlocking of hydrogen mobility at  $T_g$ , but no unlocking of oxygen mobility and is similar to the situation of onset of proton mobility in crystalline ices [113]. Because of the mobility of the H-sublattice and the purported immobility of the O-sublattice, each water molecule can switch between six conformations obeying the Bernal–Fowler rules. The possibility of a “conformational” glass transition at  $T_g$  can be ruled out on the basis of Johari’s experiment [114]: if it was a “conformational” glass transition, the sample would not be liquid above  $T_g$ , and a blunt indenter would not be able to penetrate a solid surface. Also, the high molecular mobility and isotope exchange rates measured by Kay and coworkers cannot be explained without mobility of O-atoms [115–118]. A “shadow” glass transition is a feature, which appears exclusively in hyperquenched glasses, and is well studied in hyperquenched inorganic glasses [112,119]. Such glasses show a faint step (small  $\Delta C_p$ ) preceding a much larger second step (large  $\Delta C_p$ ), corresponding to the true glass transition, in DSC thermograms. The possibility of a “shadow” glass transition in water can be ruled out because not only the hyperquenched glass of water (HGW), but also the pressure-amorphized low-density glass (LDA) and the vapor-deposited ASW show the same qualitative behavior (see Fig. 14). All three types of sample show this small  $\Delta C_p$  in spite of prior annealing (e.g., 90 min at 1 bar and 130K), which also rules out the possibility that the small  $\Delta C_p$  represents a “shadow” glass transition of an unrelaxed glass.

Highly similar DSC traces are obtained when ASW and LDA are used instead of HGW. In the case of LDA,  $T_g \sim 136\text{K}$  and  $\Delta C_p \sim 0.7\text{JK}^{-1}\text{mol}^{-1}$  (trace LDA) [102,120]. In the case of ASW,  $T_g \sim 135\text{K}$  and a slightly larger  $\Delta C_p \sim 1.9\text{JK}^{-1}\text{mol}^{-1}$  value is measured (trace ASW) [103,121]. The value of  $T_g$  obtained with ASW is consistent with isotope mixing and high diffusional- and surface mobility of water molecules observed in thin ASW films at  $T \sim 140\text{--}160\text{K}$  [115–118]. Thus,  $T_g \sim 136 \pm 2\text{K}$  for ASW, LDA, and HGW, which is consistent with the main body of experimental data [2]. In view of the barely distinguishable structure factors of ASW, LDA, and HGW and the highly similar DSC traces (see Fig. 14), all of these are connected to the same liquid state, which comes close to an ideally strong liquid rather than a fragile liquid [106,122].

In case of HDA and VHDA, the standard method of observing the glass-to-liquid transition cannot be applied at *low* pressure. For example, at 1 bar, HDA and VHDA convert to LDA at rather low temperatures of  $\sim 117\text{--}125\text{K}$ . At *high* pressures, non-standard methods are needed in order to study whether HDA and VHDA experience a reversible glass-to-liquid transition and, if so, what the pressure dependence of  $T_g$  is. This is highly nontrivial, for example, because differential scanning calorimeters operating at pressures in the GPa range and down to liquid nitrogen temperature

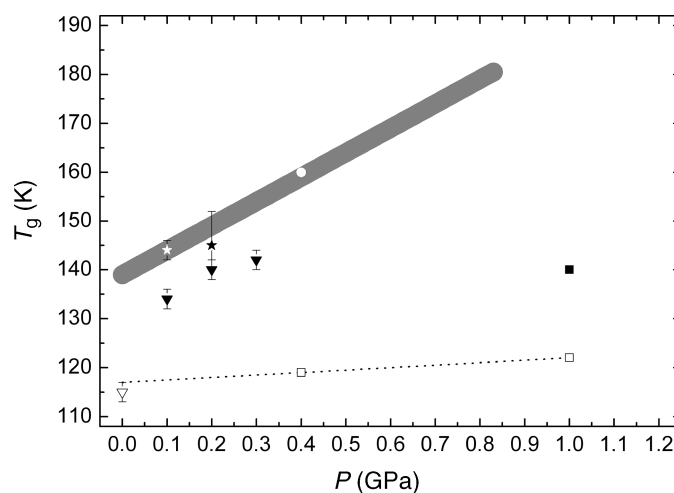


**Figure 15.** Summary of glass transition temperatures deduced in the literature as measured by Andersson et al. (squares) [80–84], Mishima (circle and grey bar) [41], Seidl et al. (triangles) [123], and Handle et al. (stars) [124]. Open squares: from dielectric relaxation measurements [80–83]; filled square: from high-pressure  $C_p$  and thermal conductivity data [84]; circle: from high-pressure DTA [41]; open triangle: by DSC at 1 bar [123]; filled triangles: by high-pressure dilatometry [123]; stars: from high-pressure structural relaxation times [124].

(77K) are barely available. Up to date, basically three groups have studied the possibility of a glass transition in HDA/VHDA. Namely the following studies have been reported: high-pressure dielectric spectroscopy [80–83], heat capacity and thermal conductivity studies on bulk water by Andersson [84], high-pressure differential thermal analysis upon decompressing emulsified VHDA by Mishima [41], and high-pressure uniaxial dilatometry of HDA by Seidl et al. [123]. Furthermore, Handle et al. have studied the relaxation of HDA as a function of time by keeping samples under isothermal and isobaric conditions [124]. All studies indicate the possibility of a glass-to-liquid transition in HDA and/or VHDA, and the glass-transition temperatures reported in these studies as a function of pressure are summarized in Fig. 15.

The dielectric relaxation times  $\tau(T)$  deduced by Andersson indicate that both VHDA at 1 GPa and HDA at 0.41 GPa are in an ultraviscous liquid state in the whole temperature range 130–160K, that is,  $T_g < 130\text{K}$ . This value of  $T_g$  is virtually unaffected by pressure [81] or shows at most a weak increase with pressure of  $5\text{K GPa}^{-1}$  according to Andersson [82]. The most recent study of VHDA's heat capacity at 1 GPa shows a step in heat capacity similar to the ones shown in Fig. 14 [82]. Andersson has deduced  $T_g$  (VHDA, 1 GPa)  $\sim 140\text{K}$  and  $\Delta C_p \sim 3.4\text{ JK}^{-1}\text{ mol}^{-1}$ ,

and crystallization at 153K [84]. This increase in heat capacity is larger than the increase for the low-density amorphous (LDA, ASW, HGW), and so Andersson has inferred the presence of liquid water under these extreme conditions (140–153K, 1 GPa). Such a  $T_g$  is surprisingly low and offers the possibility that all experiments, in which “VHDA” was studied in the past at  $P \sim 1$  GPa and  $T > 140$ K have in fact studied a liquid state, which vitrifies by quench-recovery.

Mishima reports a higher value for  $T_g$ ,  $T_g \sim 160$ K at 0.4 GPa. This value of  $T_g$  is consistent with the crossover temperature of  $\sim 160$ K at 0.4 GPa shown in Fig. 3, between melting and amorphization of ice  $I_h$  upon PIA. Mishima further assumes, based on a comparison with aqueous LiCl solutions, that the  $T_g(P)$  line follows the crystallization line, implying that  $T_g(P)$  increases at a rate of  $50 \text{ K GPa}^{-1}$  [41]. Seidl et al. have determined a similar slope of  $40 \pm 10 \text{ K GPa}^{-1}$  and  $T_g$  (HDA, 0.3 GPa)  $\sim 143$ K based on measurements of the isobaric thermal expansion behavior and its (repeatable) deviation from linearity in amorphous ice samples. By comparison with the crystallization temperature  $T_x$  and its slope of  $\sim 20 \text{ K GPa}^{-1}$ , they conclude that the glass transition temperature  $T_g$ (HDA) precedes  $T_x$ (HDA) only at pressures below 0.4 GPa, but not above 0.4 GPa. The relaxation studies of uHDA by Handle et al. from isothermal and isobaric experiments confirm that indeed long-range relaxation processes associated with dynamic properties such as diffusivity take place at 0.1 GPa and 0.2 GPa on a timescale of less than 100 s above  $T \sim 145$ K [124].

Apart from clarifying why the results in the three groups are somewhat quantitatively different, it remains to be explored in the future whether HDA and VHDA show different  $T_g(P)$  characteristics, as suggested from the currently available data.

## XI. DISCUSSION

In this chapter, we reviewed the phenomenology of water in the glassy state. Three amorphous ices were identified, namely LDA, HDA, and VHDA. The different recipes of preparation of these amorphous ices, the structure of these glasses, as well as the relationship between them were discussed in detail. A brief summary of the glass transition phenomenology of the different amorphous ices was also included.

One of the more relevant questions related to amorphous ices is probably how to quantify the number of known amorphous states. From the structural point of view, one can identify three amorphous ices, namely LDA, HDA, and VHDA. Both experiments and computer simulations indicate that the structure of these amorphous ices is characterized by the absence of long-range order beyond 10–20 Å and by local tetrahedral coordination, in agreement with the Walrafen pentamer geometry. Thus, in all these amorphous ices, the arrangement of a water molecule and its four nearest neighbors is not different from ice and the Bernal–Fowler rules

[125], originally developed to describe ice local hydrogen bonding in crystalline ice, also apply for LDA, HDA, and VHDA. The main difference in the structure of LDA, HDA, and VHDA is in the number of molecules in the first interstitial shell [56,85]. In the case of LDA, water molecules have no neighbor molecules in their first interstitial shell. Instead, one and two such interstitial molecules are present in the case of HDA and VHDA, respectively. These interstitial molecules form no direct hydrogen bond with a given central water molecule and represent defects in water tetrahedral hydrogen-bond network. The different packing results in significant different densities; at 1 bar and 77K, HDA is 25% denser than LDA and VHDA is 9% denser than HDA. From the thermodynamics point of view, the distinction between LDA, HDA, and VHDA is less clear. Part of the difficulty in identifying amorphous ices relies on how one defines an amorphous solid state. While there is a single structure associated with a crystal, the structure of an amorphous solid may differ slightly depending on the specific route followed in the experiment, compression, and/or heating rates. Furthermore, the structure of amorphous solids can change upon aging or annealing. For example, the HDA structure changes slightly upon heating at 1 bar [43,45–48,126,127], before transforming into LDA. If the particular structure of the amorphous ice, as defined, for example, by its neutron diffraction pattern, is used to define an amorphous “state,” then one should conclude that an infinite number of amorphous solids exist in water. This definition is rather misleading since it would imply that most substances also show “polyamorphism.”

A better way to identify different amorphous states is clearly needed. One possibility is to consider that amorphous states are separated by “first-order-like transitions,” that is, by *discontinuous* changes in thermodynamics properties, such as sudden pressure changes along isothermal compression/decompression paths or temperature changes along isobaric heating/cooling paths [64]. These transformations between different amorphous solids must also be reversible in some temperature–pressure range and must be accompanied by coexistence of the amorphous solids in a single sample [67,92]. Otherwise, the sudden change in thermodynamic properties could be a result of sudden relaxation in a single amorphous solid. Using this definition of amorphous state, one would conclude that two different amorphous states exist in water, LDA, and HDA. VHDA, although distinct in structure from HDA, would be a relaxed form of HDA; the corresponding relaxation process being sudden and occurring in a narrow region of the  $P$ – $T$  plane [65,66]. However, an important caveat inherent to this definition is provided by the nonequilibrium nature defining the amorphous state. A structural (or enthalpy) relaxation toward more stable amorphous states is always superimposed on the transition, and the question always remains whether a transition that appears sharp and discontinuous is in fact sharp, but continuous. Therefore, some researchers think that all amorphous ices (LDA, HDA, and VHDA) are continuously connected. Alternatively, it is also possible that a transition, which is continuous in

appearance, represents in fact a first-order transition that is smeared by relaxation effects, and would appear as a discontinuous transition only at higher temperature. In principle, it would be even possible that a continuous transition, such as the HDA–VHDA transformation, represents a supercritical transition, and would show a discontinuous nature at lower temperature (below the critical temperature), probably deep into the glass domain.

An alternative criterion to identify different amorphous states (circumventing the issue of superimposed equilibration) is to consider that transformations between amorphous solids are accompanied by sudden, but not necessarily discontinuous, changes in thermodynamic properties (which occur at reproducible values of pressure and temperature). These transformations must also be reversible, but not necessarily accompanied by coexistence of two distinct amorphous ices. Since the amorphous states are different, these amorphous solids should also have different thermodynamic properties, such as heat capacity and compressibility. Figure 11 indicates that HDA and VHDA have different compressibilities in the pressure range 0.3–1.9 GPa, namely  $0.20 \text{ g cm}^{-3} \text{ GPa}^{-1}$  at  $P < 0.8 \text{ GPa}$  and  $0.14 \text{ g cm}^{-3} \text{ GPa}^{-1}$  at  $P > 0.8 \text{ GPa}$ , respectively. Using this criterion to identify different amorphous states, one must conclude that water is characterized by three amorphous ices, LDA, HDA, and VHDA. This criterion is implicit in the IUPAP definition of “phases” and has also been employed to define polyamorphic states connected by continuous transitions in other systems such as  $\text{SiO}_2$ ,  $\text{GeO}_2$ , or Si [128]. Also the pressure-dependence of the glass transition temperature may be used as a criterion. LDA and HDA clearly show different glass transition temperatures [123], and recent high-pressure studies also suggest that  $T_g(P)$  might differ for HDA and VHDA [41,83,84,123]. We wish to emphasize that this is consistent with the observation that there are only two homogeneous amorphous ice structures at 1 bar [129] since high pressures are required to “separate” HDA and VHDA.

Independently of the definition of “amorphous polymorphism” chosen, experiments suggest that the relationship between LDA and HDA (“first-order like”) is different from the relationship between HDA and VHDA (“continuous”), at least at 140K [65,66]. Therefore, the possibility that there exists a second critical point in metastable water within the “No man’s land” is still open and remains the topic for future works. However, the continuous nature of the HDA–VHDA transformation strongly questions the possibility of a third critical point in metastable water. Experiments at slower compression/decompression rates and at higher temperatures ( $>140\text{K}$ ) may help to elucidate this issue.

While the glass transition temperature of LDA is  $T_g(1 \text{ bar}) \sim 136\text{K}$ , it is an open question what the value of  $T_g(P)$  is for LDA, HDA, and VHDA at high pressure. The first few experiments reporting such data at high pressure are summarized in Fig. 15. At ambient pressure, the LDA-like glasses, ASW and HGW, have shown to be continuously thermodynamically connected to a low-density liquid of “strong” nature in the range 136–150K (Fig. 14). All these experiments point in the

direction that LDA, HDA, and VHDA are indeed connected to deeply supercooled liquids. Yet, more experiments are clearly needed to answer the open questions [36,130,131]. One strategy of resolving some of the controversies might be to redo some of the experiments performed on uHDA in the past on eHDA. So, it still remains to be clarified in the future whether or not “polyamorphism” is related to liquid–liquid transitions in the one-component system water, and whether or not such transitions between two liquids differing by 25% in density are at the origin of liquid water’s anomalies.

### ACKNOWLEDGMENTS

K. W. and T. L. are thankful to the Austrian Science Fund FWF for their continuous support and to the European Research Council (ERC Starting Grant SULIWA). ~~N. G. thanks The City University of New York for support (PSC-CUNY Research Award Program).~~ We are grateful to Erwin Mayer for reading and commenting the manuscript before his untimely death.

### REFERENCES

1. M. Chaplin, ~~(2011)~~
2. P. G. Debenedetti, *J. Phys. Condens. Matter* **15**, R1669 (2003).
3. K. Röttger, A. Endriss, J. Ihringer, S. Doyle, and W. F. Kuhs, *Acta Crystallogr.* **B50**, 644 (1994).
4. H. E. Stanley, *Pramana* **53**, 53 (1999).
5. H. E. Stanley, S. V. Buldyrev, M. Canpolat, O. Mishima, M. R. Sadr-Lahijany, A. Scala, and F. W. Starr, *Phys. Chem. Chem. Phys.* **2**, 1551 (2000).
6. C. A. Angell, *Annu. Rev. Phys. Chem.* **55**, 559 (2004).
7. T. Loerting and N. Giovambattista, *J. Phys. Condens. Matter* **18**, R919 (2006).
8. G. P. Johari and O. Andersson, *Thermochim. Acta* **461**, 14 (2007).
9. D. Ganguli, *Trans. Indian Ceram. Soc.* **68**, 65 (2009).
10. G. Malenkov, *J. Phys. Condens. Matter* **21**, 283101/1 (2009).
11. S. C. Mossop, *Proc. Phys. Soc. B* **68**, 193 (1955).
12. C. A. Angell, J. Shuppert, and J. C. Tucker, *J. Phys. Chem.* **77**, 3092 (1973).
13. H. Kanno, R. J. Speedy, and C. A. Angell, *Science* **189**, 880 (1975).
14. W. Kauzmann, *Chem. Rev.* **43**, 219 (1948).
15. T. Ichitsubo, E. Matsubara, H. Numakura, K. Tanaka, N. Nishiyama, and R. Tarumi, *Phys. Rev. B* **72**, 052201/1 (2005).
16. J. Swenson, R. Bergman, and S. Longeville, *J. Non-Cryst. Solids* **573**, 307–310, (2002).
17. F. Mallamace, M. Broccio, C. Corsaro, A. Faraone, U. Wanderlingh, L. Liu, C. Y. Mou, and S. H. Chen, *J. Chem. Phys.* **124**, 161102/1 (2006).
18. J. M. Zanotti, M. C. Bellissent-Funel, and S. H. Chen, *Europhys. Lett.* **71**, 91 (2005).
19. S. H. Chen, L. Liu, X. Chu, Y. Zhang, E. Fratini, P. Baglioni, A. Faraone, and E. Mamontov, *J. Chem. Phys.* **125**, 171103/1 (2006).

Q1

20. J. Swenson, H. Jansson, and R. Bergman, *Phys. Rev. Lett.* **96**, 247802/1 (2006).
21. T. Loerting, K. Winkel, M. Seidl, M. Bauer, C. Mitterdorfer, P. H. Handle, C. G. Salzmann, E. Mayer, J. L. Finney, and D. T. Bowron, *Phys. Chem. Chem. Phys.* **13**, 8783 (2011).
22. C. G. Salzmann, T. Loerting, S. Klotz, P. W. Mirwald, A. Hallbrucker, and E. Mayer, *Phys. Chem. Chem. Phys.* **8**, 386 (2006).
23. C. G. Salzmann, P. G. Radaelli, E. Mayer, and J. L. Finney, *Phys. Rev. Lett.* **103**, 105701/1 (2009).
24. O. Mishima, L. D. Calvert, and E. Whalley, *Nature* **310**, 393 (1984).
25. E. G. Ponyatovskii and O. I. Barkalov, *Mater. Sci. Rep.* **8**, 147 (1992).
26. S. Kawasaki, O. Ohtaka, and T. Yamanaka, *Phys. Chem. Miner.* **20**, 531 (1994).
27. A. Grzechnik, T. Grande, and S. Stolen, *J. Solid State Chem.* **141**, 248 (1998).
28. S. K. Deb, M. Wilding, M. Somayazulu, and P. F. McMillan, *Nature* **414**, 528 (2001).
29. R. J. Hemley, A. P. Jephcoat, H. K. Mao, L. C. Ming, and M. H. Manghnani, *Nature* **334**, 52 (1988).
30. R. J. Hemley, L. C. Chen, and H. K. Mao, *Nature* **338**, 638 (1989).
31. S. Klotz, G. Hamel, J. S. Loveday, R. J. Nelmes, and M. Guthrie, *Z. Kristallogr.* **218**, 117 (2003).
32. T. Loerting, M. Bauer, I. Kohl, K. Watschinger, K. Winkel, and E. Mayer, *J. Phys. Chem. B* **115**, 14167 (2011).
33. O. Mishima, L. D. Calvert, and E. Whalley, *J. Phys. Colloq.* **C8**, 239 (1984).
34. O. Mishima, *J. Chem. Phys.* **115**, 4199 (2001).
35. J. S. Tse, *J. Chem. Phys.* **96**, 5482 (1992).
36. J. S. Tse, D. D. Klug, C. A. Tulk, I. Swainson, E. C. Svensson, C.-K. Loong, V. Shpakov, V. R. Belosludov, R. V. Belosludov, and Y. Kawazoe, *Nature* **400**, 647 (1999).
37. O. Mishima, *Nature* **384**, 546 (1996).
38. A. G. Lyapin, O. V. Stal'gorova, E. L. Gromnitskaya, and V. V. Brazhkin, *J. Exp. Theor. Phys.* **94**, 283 (2002).
39. G. P. Johari and O. Andersson, *J. Chem. Phys.* **120**, 6207 (2004).
40. M. Bauer, M. S. Elsaesser, K. Winkel, E. Mayer, and T. Loerting, *Phys. Rev. B* **77**, 220105/1 (2008).
41. O. Mishima, *J. Chem. Phys.* **121**, 3161 (2004).
42. R. J. Nelmes, J. S. Loveday, T. Straessle, C. L. Bull, M. Guthrie, G. Hamel, and S. Klotz, *Nat. Phys.* **2**, 414 (2006).
43. C. A. Tulk, C. J. Benmore, J. Urquidi, D. D. Klug, J. Neufeind, B. Tomberli, and P. A. Egelstaff, *Science* **297**, 1320 (2002).
44. M. Guthrie, J. Urquidi, C. A. Tulk, C. J. Benmore, D. D. Klug, and J. Neufeind, *Phys. Rev. B* **68**, 184110 (2003).
45. M. M. Koza, H. Schober, H. E. Fischer, T. Hansen, and F. Fujara, *J. Phys. Condens. Matter* **15**, 321 (2003).
46. M. M. Koza, B. Geil, K. Winkel, C. Koehler, F. Czeschka, M. Scheuermann, H. Schober, and T. Hansen, *Phys. Rev. Lett.* **94**, 125506 (2005).
47. E. L. Gromnitskaya, O. V. Stal'gorova, V. V. Brazhkin, and A. G. Lyapin, *Phys. Rev. B* **64**, 094205 (2001).
48. Y. P. Handa, O. Mishima, and E. Whalley, *J. Chem. Phys.* **84**, 2766 (1986).
49. E. F. Burton and W. F. Oliver, *Nature* **135**, 505 (1935).
50. C. G. Venkatesh, S. A. Rice, and A. H. Narten, *Science* **186**, 927 (1974).

51. P. Jenniskens and D. F. Blake, *Science* **265**, 753 (1994).
52. P. Brüggeller and E. Mayer, *Nature* **288**, 569 (1980).
53. E. Mayer, *J. Appl. Phys.* **58**, 663 (1985).
54. I. Kohl, L. Bachmann, A. Hallbrucker, E. Mayer, and T. Loerting, *Phys. Chem. Chem. Phys.* **7**, 3210 (2005).
55. J. Dubochet and A. W. McDowell, *J. Microsc.* **124**, RP3 (1981).
56. J. L. Finney, A. Hallbrucker, I. Kohl, A. K. Soper, and D. T. Bowron, *Phys. Rev. Lett.* **88**, 225503 (2002).
57. D. T. Bowron, J. L. Finney, A. Hallbrucker, I. Kohl, T. Loerting, E. Mayer, and A. K. Soper, *J. Chem. Phys.* **125**, (2006).
58. Y. Suzuki and O. Mishima, *J. Phys. Soc. Jpn.* **72**, 3128 (2003).
59. C. A. Tulk, D. D. Klug, R. Branderhorst, P. Sharpe, and J. A. Ripmeester, *J. Chem. Phys.* **109**, 8478 (1998).
60. O. Mishima and H. E. Stanley, *Nature* **396**, 329 (1998).
61. K. Winkel, D. T. Bowron, T. Loerting, E. Mayer, and J. L. Finney, *J. Chem. Phys.* **130**, 204502 (2009).
62. O. Mishima, L. D. Calvert, and E. Whalley, *Nature* **314**, 76 (1985).
63. C. T. Moynihan, *Ann. N. Y. Acad. Sci.* **484**, 94 (1986).
64. O. Mishima, *J. Chem. Phys.* **100**, 5910 (1994).
65. K. Winkel, M. S. Elsaesser, E. Mayer, and T. Loerting, *J. Chem. Phys.* **128**, 044510/1 (2008).
66. K. Winkel, M. S. Elsaesser, M. Seidl, M. Bauer, E. Mayer, and T. Loerting, *J. Phys. Condens. Matter* **20**, 494212 (2008).
67. O. Mishima, K. Takemura, and K. Aoki, *Science* **254**, 406 (1991).
68. K. Winkel, E. Mayer, and T. Loerting, *J. Phys. Chem. B* **115**, 14141 (2011).
69. K. Winkel, *Study of Amorphous–Amorphous Transitions in Water*, Verlag Dr. Hut, Munich, 2011.
70. S. Klotz, T. Straessle, R. J. Nelmes, J. S. Loveday, G. Hamel, G. Rousse, B. Canny, J. C. Chervin, and A. M. Saitta, *Phys. Rev. Lett.* **94**, 025506 (2005).
71. Y. Yoshimura, S. T. Stewart, H.-K. Mao, and R. J. Hemley, *J. Chem. Phys.* **126**, (2007).
72. J. S. Tse and M. L. Klein, *Phys. Rev. Lett.* **58**, 1672 (1987).
73. J. S. Tse and M. L. Klein, *J. Chem. Phys.* **92**, 3992 (1990).
74. E. Whalley, D. D. Klug, and Y. P. Handa, *Nature* **342**, 782 (1989).
75. P. H. Poole, F. Sciortino, U. Essmann, and H. E. Stanley, *Nature* **360**, 324 (1992).
76. O. Mishima and H. E. Stanley, *Nature* **392**, 164 (1998).
77. H. B. Callen, *Thermodynamics and an Introduction to Thermostatistics*, 2nd ed., John Wiley & Sons, Inc., New York, 1985.
78. T. Loerting, C. Salzmann, I. Kohl, E. Mayer, and A. Hallbrucker, *Phys. Chem. Chem. Phys.* **3**, 5355 (2001).
79. T. Loerting, W. Schustereder, K. Winkel, C. G. Salzmann, I. Kohl, and E. Mayer, *Phys. Rev. Lett.* **96**, 025702 (2006).
80. G. P. Johari and O. Andersson, *NATO Sci. Ser., II* **242**, 35 (2007).
81. O. Andersson, *Phys. Rev. Lett.* **95**, 205503 (2005).
82. O. Andersson and A. Inaba, *Phys. Rev. B* **74**, (2006).
83. O. Andersson, *J. Phys. Condens. Matter* **20**, 244115 (2008).

84. O. Andersson, *Proc. Natl. Acad. Sci. USA* **108**, 11013 (2011).
85. J. L. Finney, D. T. Bowron, A. K. Soper, T. Loerting, E. Mayer, and A. Hallbrucker, *Phys. Rev. Lett.* **89**, 205503 (2002).
86. J. A. Ripmeester, C. I. Ratcliffe, and D. D. Klug, *J. Chem. Phys.* **96**, 8503 (1992).
87. N. Giovambattista, H. Eugene Stanley, and F. Sciortino, *Phys. Rev. E* **72**, 031510 (2005).
88. R. Martonak, D. Donadio, and M. Parrinello, *J. Chem. Phys.* **122**, 134501 (2005).
89. R. Martonak, D. Donadio, and M. Parrinello, *Phys. Rev. Lett.* **92**, 225702 (2004).
90. N. Giovambattista, H. E. Stanley, and F. Sciortino, *Phys. Rev. Lett.* **94**, 107803 (2005).
91. Y. Suzuki and O. Mishima, *J. Phys. Condens. Matter* **21**, 155105/1 (2009).
92. S. Klotz, T. Straessle, A. M. Saitta, G. Rousse, G. Hamel, R. J. Nelmes, J. S. Loveday, and M. Guthrie, *J. Phys. Condens. Matter* **17**, S967 (2005).
93. P. H. Poole, U. Essmann, F. Sciortino, and H. E. Stanley, *Phys. Rev. E* **48**, 4605 (1993).
94. D. Paschek, A. Ruppert, and A. Geiger, *Chem. Phys. Chem.* **9**, 2737 (2008).
95. I. Brovchenko, A. Geiger, and A. Oleinikova, *J. Chem. Phys.* **118**, 9473 (2003).
96. I. Brovchenko, A. Geiger, and A. Oleinikova, *J. Chem. Phys.* **123**, 044515 (2005).
97. P. Jedlovsky and R. Vallauri, *J. Chem. Phys.* **122**, 081101/1 (2005).
98. S. V. Buldyrev and H. E. Stanley, *Physica A* **330**, 124 (2003).
99. C. W. Hsu, J. Largo, F. Sciortino, and F. W. Starr, *Proc. Natl. Acad. Sci. USA* **105**, 13711 (2008).
100. Y. Liu, A. Z. Panagiotopoulos, and P. G. Debenedetti, *J. Chem. Phys.* **131**, 104508 (2009).
101. G. P. Johari, A. Hallbrucker, and E. Mayer, *Nature* **330**, 552 (1987).
102. A. Hallbrucker, E. Mayer, and G. P. Johari, *J. Phys. Chem.* **93**, 4986 (1989).
103. C. G. Salzmann, I. Kohl, T. Loerting, E. Mayer, and A. Hallbrucker, *Phys. Chem. Chem. Phys.* **5**, 3507 (2003).
104. I. Kohl, L. Bachmann, E. Mayer, A. Hallbrucker, and T. Loerting, *Nature* **435**, E1 (2005).
105. A. Minoguchi, R. Richert, and C. A. Angell, *Phys. Rev. Lett.* (2004).
106. S. M. McClure, D. J. Safarik, T. M. Truskett, C. B. Mullins, *J. Phys. Chem. B* **110**, 11033 (2006).
107. C. A. Angell, *J. Phys. Condens. Matter* **19**, 205112/1 (2007).
108. S. Capaccioli and K. L. Ngai, *J. Chem. Phys.* **135**, 104504/1 (2011).
109. C. A. Angell, *Chem. Rev.* **102**, 2627 (2002).
110. K. Ito, C. T. Moynihan, and C. A. Angell, *Nature* **398**, 492 (1999).
111. M. Fisher and J. P. Devlin, *J. Phys. Chem.* **99**, 11584 (1995).
112. Y. Yue and C. A. Angell, *Nature* **427**, 717 (2004).
113. C. G. Salzmann, P. G. Radaelli, B. Slater, and J. L. Finney, *Phys. Chem. Chem. Phys.* **13**, 18468 (2011).
114. G. P. Johari, *J. Phys. Chem. B* **102**, 4711 (1998).
115. A. Stintz and J. A. Panitz, *Surf. Sci.* **296**, 75 (1993).
116. A. Stintz and J. A. Panitz, *Int. J. Mass Spectrom. Ion Processes* **133**, 59 (1994).
117. R. S. Smith and B. D. Kay, *Nature* **398**, 788 (1999).
118. R. S. Smith, Z. Dohnalek, G. A. Kimmel, K. P. Stevenson, and B. D. Kay, *Chem. Phys.* **258**, 291 (2000).
119. Y. Z. Yue, S. L. Jensen, and J. d. Christiansen, *Appl. Phys. Lett.* **81**, 2983 (2002).
120. Y. P. Handa and D. D. Klug, *J. Phys. Chem.* **92**, 3323 (1988).

121. J. A. McMillan and S. C. Los, *Nature* **206**, 806 (1965).
122. M. Chonde, M. Brindza, and V. Sadtschenko, *J. Chem. Phys.* **125**, 094501/1 (2006).
123. M. Seidl, M. S. Elsaesser, K. Winkel, G. Zifferer, E. Mayer, and T. Loerting, *Phys. Rev. B Condens. Matter Mater. Phys.* **83**, 100201/1 (2011).
124. P. H. Handle, M. Seidl, and T. Loerting, ~~prepared for submission (2011)~~ **Q2**
125. J. D. Bernal and R. H. Fowler, *J. Chem. Phys.* **1**, 515 (1933).
126. O. V. Stal'gorova, E. L. Gromnitskaya, V. V. Brazhkin, and A. G. Lyapin, *JETP Lett. (Translation of Pis'ma v Zhurnal Eksperimental'noi i Teoreticheskoi Fiziki)* **69**, 694 (1999).
127. J. S. Tse, D. D. Klug, M. Guthrie, C. A. Tulk, C. J. Benmore, and J. Urquidi, *Phys. Rev. B* **71**, 214107 (2005).
128. T. Loerting, V. V. Brazhkin, and T. Morishita, *Adv. Chem. Phys.* **143**, 29 (2009).
129. M. M. Koza, T. Hansen, R. P. May, and H. Schober, *J. Non-Cryst. Solids* **352**, 4988 (2006).
130. H. Schober, M. M. Koza, A. Tolle, C. Masciovecchio, F. Sette, and F. Fujara, *Phys. Rev. Lett.* **85**, 4100 (2000).
131. M. M. Koza, H. Schober, B. Geil, M. Lorenzen, and H. Requardt, *Phys. Rev. B* **69**, 024204/1 (2004).

**Author Queries**

- Q1** Please provide complete details in Ref. [1].
- Q2** Please update Ref. [124].

UNCORRECTED PROOF